Benefits of Nitric Oxide Cues to Matrix Synthesis by Healthy and Aneurysmal Human Smooth Muscle Cells within 3D Cocultures

PHILLIP SIMMERS

Bachelor of Science in Biomedical Engineering

University of Cincinnati

June 2012

Submitted in partial fulfillment of requirements for the degree

MASTER OF SCIENCE IN BIOMEDICAL ENGINEERING

at

CLEVELAND STATE UNIVERSITY

May 2014

We hereby approve this thesis of

Phillip Simmers

Candidate for the Master of Science in Biomedical Engineering degree for the

Department of Chemical and Biomedical Engineering

And the CLEVELAND STATE UNIVERSITY
College of Graduate Studies

Thesis Chairperson, Dr. Chandra Kothapalli
Department of Chemical and Biomedical Engineering

_____
Date

Thesis Committee Member, Dr. Nolan Holland
Department of Chemical and Biomedical Engineering

_____
Date

Thesis Committee Member, Dr. Moo-Yeal Lee
Department of Chemical and Biomedical Engineering

_____
Date

Thursday, May 1, 2014

ACKNOWLEDGMENTS

First and foremost I would like to thank my advisor, Dr. Chandra Kothapalli for his support and council. Dr. Kothapalli's belief and trust in my abilities as well as his instruction and experience in cardiovascular tissue engineering studies was essential in the completion of this thesis. I would also like to acknowledge my committee members, Dr. Nolan B. Holland and Dr. Moo-Yeal Lee for their time and support.

The assistance and support received from my fellow colleagues at Cleveland State University was greatly appreciated. Specifically I would like to thank Mike Sawonik and James Deyling in their assistance in the design and fabrication of microfluidic devices. I would also like to mention Kurt Farrell for his help in training me in many of the common laboratory procedures, assisting in the experimental execution, as well as his guidance. A special thanks to Arsela Gishto, who assisted and instructed me on many of the experimental procedures in the lab. I would also like to acknowledge my fellow lab members, Jyotsna Joshi, Amanda Powell, and Sameera Tasneem for their continued support. Finally, this work would never be possible without the Chemical and Biomedical Engineering staff at Cleveland State University, especially Becky Laird and Darlene Montgomery.

The continued support from Microfluidics Foundry at Stanford University in the creation of the device molds is greatly appreciated. The financial support provided by the Choose Ohio First Scholarship under the direction of Dr. Jorge E. Gatica as well as the graduate assistant position given by Dr. Petru S. Fodor and Dr. Andrew H. Resnick and teaching assistant provided by Dr. Rolf Lustig is greatly appreciated. Thanks is also given to the faculty Research Development Award, Provost Undergraduate Research and

Creative Achievement Award (2012-2013 Cleveland State University), and the NSF grant (1337859) for providing the necessary funds to perform some of the experiments.

Lastly, I would like to acknowledge my family members. Specifically, my mother, Mary Pat Simmers, my father, Scott Simmers, and my sister, Lorainne Simmers, for their continued love and support. I would also like to acknowledge my grandparents, specifically my grandfather, Kenneth E. Simmers, as he unknowingly motivated me to pursue a degree in biomedical engineering.

Benefits of Nitric Oxide Cues to Matrix Synthesis by Healthy and Aneurysmal Human Smooth Muscle Cells within 3D Cocultures

PHILLIP SIMMERS

ABSTRACT

Vascular diseases such as atherosclerosis and aneurysms are characterized by the over-proliferation and migration of aortic smooth muscle cells (SMCs), and degradation of extracellular matrix (ECM) within the vessel wall, leading to compromise in cell-cell and cell-matrix signaling pathways. Recent tissue engineering approaches to regulate SMC over-proliferation and enhance healthy ECM synthesis showed promise, but resulted in low crosslinking efficiency and matrix deposition yields. In this study, the benefits of exogenous nitric oxide cues, delivered from S-Nitrosoglutathione (GSNO), to cell proliferation and matrix deposition by adult human aortic SMCs (HA-SMCs) within 3D biomimetic cultures have been explored. The first experiment utilized a microfluidic platform with two adjacent, permeable 3D culture chambers, to enable paracrine signaling between vascular cell cocultures. Healthy HA-SMCs were cultured in these devices within 3D collagen hydrogels, either alone or in the presence of human aortic endothelial cell (HA-ECs) cocultures, and exogenously supplemented with varying GSNO dosages (0-100 nM) for 21 days. Results showed that EC cocultures stimulated SMC proliferation within GSNO-free cultures. However, with increasing GSNO concentration, HA-SMC proliferation decreased in the presence or absence of EC cocultures, while HA-EC proliferation increased. GSNO (100 nM) significantly enhanced the total protein amount synthesized by HA-SMCs, in the presence or absence of EC

cocultures, while lower dosages (1-10 nM) offered marginal benefits. On a per cell basis, multi-fold increases in the synthesis and deposition of elastin, glycosaminoglycans, hyaluronic acid and lysyl oxidase crosslinking enzyme (LOX) were noted at higher GSNO dosages, and coculturing with ECs significantly furthered these trends. The matrix yields of these proteins reached almost 40 - 51 % within selective cocultures receiving GSNO. Similar increases in TIMP-1 and MMP-9 levels were noted within cocultures with increasing GSNO dosages, although MMP-2 levels remained attenuated. These quantitative assay data were strongly supported by immunofluorescence images under respective conditions. Based on the optimized dosage (100 nM) deduced from first experiment, we tested the utility of NO cues within diseased HA-SMC (derived from aneurysmal human aortic segment) cultures, under both 2D and 3D culture conditions. Results showed that cell proliferation was higher on 2D substrates compared to that within 3D cultures. In accordance to the trends noted within healthy SMC cultures, there was a decrease in cell proliferation in both 2D and 3D, with increasing GSNO dose. Similarly, the presence of GSNO stimulated elastin, glycosaminoglycans, hyaluronic acid, lysyl oxidase crosslinking enzyme (LOX), MMP-2, 9 and TIMP-1 synthesis and release by aneurysmal SMCs, although the matrix deposition levels were lower compared to their healthy counterparts. Both experiments results attest to the tremendous benefits of delivering nitric oxide cues to suppress SMC proliferation and promote robust ECM synthesis and deposition by adult human SMCs, with significant applications in tissue engineering, biomaterial scaffold development, and drug delivery.

TABLE OF CONTENTS

Page

LIST OF TABLES

LIST OF FIGURES

CHAPTER I

BACKGROUND

1.1. Vascular tissue organization

Excluding the capillaries and the venules of the peripheral circulation system, all blood vessel walls are composed of three distinct layers: tunica intima, tunica media, and the tunica adventitia (**Fig. 1.1**). The tunica intima is the inner most layer, which is composed of endothelium and a connective tissue basement membrane. Following the basement membrane is a layer of smooth muscle and connective tissue called the lamina propria. Encapsulating the lamina propria is the internal elastic membrane, which consist primarily of elastic fibers. Following the tunica intima is the tunica media which is a layer of smooth muscle cells with a circular arrangement. This is the layer that allows for the movement of blood through the vessel through contraction and relaxation. Just like the outer layer of the tunica intima the tunica media has an elastic membrane that separates it from the tunica adventitia. The last layer, or the tunica adventitia, is

composed of dense connective tissue near the tunica media and gradually transitions to loose connective tissue in order to merge the blood vessels with the surrounding tissue[1].

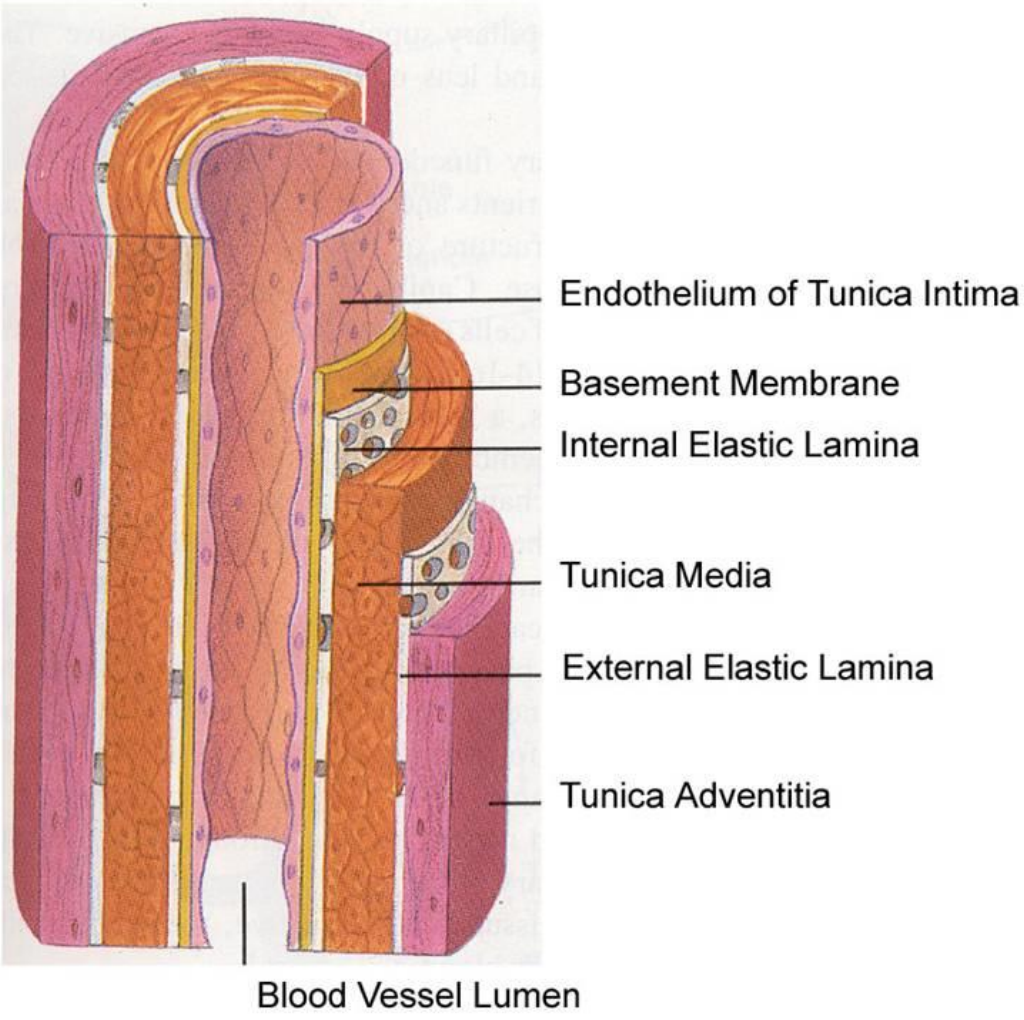

Figure 1.1 The layers of the blood vessel[2].

1.2. Vascular extracellular matrix

Vascular tissue as described previously is broken up into three different layers. The composition of the extracellular matrix adds to the overall properties of the individual layers and is dependent on the cell phenotype located in the layer. The tunica intima

connective tissue is very thin and primarily made of endothelial cells with little matrix while the smooth muscle cells in the tunica media deposit and upkeep the internal and external elastic lamina which are responsible for the pulsatile stretching forces experienced in the arterial walls. Lastly, the fibroblast located in the tunica adventitia deposit much of the collagen found in the vascular tissue[1]. The description of the most important extracellular matrix proteins of the vascular tissue can be found below.

1.2.1. Collagen

The most abundant protein found in ECM is collagen which plays an integral role in providing both support and tensile strength to the vascular tissue. Collagen exists in many different types in the human body, but the most common one found in vascular tissue is type I, which comprises 80% of the total collagen found. Type III makes up 12% of collagen found with the last 8% being composed of trace concentrations of types IV, V, and VI collagen. The structure of all collagen is that of a triple helix that are constructed with α-chains. It is the altercations in the α-chains that result in the formation of different collagen types. The glue that holds the triple helix structure of collagen together is the chemical bonds between the hydroxylated amino acids of proline and lysine. The fibrous nature of collagen I, III, and V aggregates together to create larger fibers. These fibers are the main structural support of the tissue and connect main vascular tissue components[3–8]. Cells are able to migrate along the collagen fiber through the use of fibronectin[9].

1.2.2. Glycosaminoglycans

Glycosaminoglycans (GAGs) are anionic polysaccharides with hydrophilic chains that have many disaccharide units. There are two main types of GAGs, those with and those without sulfated groups attached to the sugar molecules. Further categorization of GAGs focuses not only on sulfate groups, but the types of sugars and their bonding characteristics. The four main groups of GAGs are; hyaluronan, chondroitin sulfate, heparin sulfate, and keratin sulfate. The only GAG that is non-sulfated in its disaccharide unit is the hyaluronic acid (HA) molecules[4,6,10].

GAGs are known mainly for their hydrophilic properties that allow them to expand forming hydrogels. This occurs by the large negative charges on their surface, which attract many cations that are osmotically active, to successfully attract water into the GAG matrix. Mechanically, GAGs are resistant to compression and thus help vascular tissue to keep its physical integrity from exterior forces. Also sulfated GAGs are able to covalently bond to other proteins, which form structures commonly known are proteoglycans[9].

Proteoglycans perform a wide range of functions for the surrounding cells. One proteoglycan unit consists of a protein core attached to covalently bonded GAG chains. They provide the necessary hydrated space around cells, regulate the passage of certain molecules, bind to growth factors and other signaling proteins for signal transduction, and guide cell migration through the extracellular matrix[9].

1.2.3. Elastin

One of the most essential ECM protein of the vascular system, elastin provides the necessary elastic properties allowing for blood to be properly pumped through the circulatory system by bearing the mechanical pressure applied to the tissue during the cardiac cycle[9]. Elastin is formed when soluble monomers, tropoelastin and fibrillin, are cross-linked by the enzyme lysyl oxidase (LOX) forming an insoluble protein. Fibrillin is a glycoprotein that is essential in the formation of elastic fibers. Each type of fibrillin performs a different function in the formation of fibers with fibrillin-I performing the most important function in elastin formation. Fibrillin-1 serves as a structure glue component of calcium by binding microfibrils (i.e. tropoelastin). The microfibrils then provide the structural integrity of tissues as well regulation of cytokines through the sequestration of molecules. The majority of elastin is synthesized during the neonatal developing stages, or the period from birth to one month old, and there is a significant decrease in the synthesis of mature matrix elastin in adults. Elastin is not only important due to the mechanical properties it contributes to the overall tissue but it has been also noted to regulate SMC proliferation and morphology[11–14] .

1.2.4. Lysyl oxidases

Lysyl oxidases (LOX) are an extracellular copper enzyme that can catalyze aldehydes from lysine residues in tropocollagen and tropoelastin. The aldehydes are highly reactive and thus spontaneously react with lysyl oxidase derived aldehyde residues resulting in the cross-linking of collagen and elastin, which successfully stabilizes the collagen fibrils as well as develops mature matrix elastin[15] .

1.2.5. Matrix metalloproteinases and their inhibitors

Matrix metalloproteinases (MMPs) are naturally occurring extracellular proteolytic enzymes that degrade ECM proteins. During periods of inflammation these enzymes are upregulated in order to destroy the ECM to make room for inflammatory cells. MMPs are able to break down much of the ECM proteins by attacking the cross-linkers that hold many of the proteins together. To ensure that MMPs are not left unchecked, the synthesis of tissue inhibitors of metalloproteinases (TIMPs) is necessary for protection of non-damaged tissue. TIMPs are protease–specific and bind to activated proteases during the inflammatory phase restricting the activity of MMPs[6,8] . Thus, a careful balance of both TIMP and MMP expression is needed to properly reorganize vascular ECM.

1.3. Vascular aneurysm

When vascular elastin is congenitally malformed, or damaged by local injury, or degraded by acquired diseases, it severely compromises vessel integrity, disrupts cellular signaling pathways, initiates inflammation, and weakens vessel wall[16]. This can lead to an aneurysm or the ballooning/dilation of an artery. Aneurysms can come in two general shapes as seen in **Fig.1.2**. The first is the formation of a pouch or sac on one side of the blood vessel wall and is commonly known as a saccular aneurysm. The second is called the fusiform aneurysm and is commonly defined as the dilation of the artery in all directions[17]. Hypertension of this area can lead to a burst in the vessel and thus hemorrhage of blood into the surrounding tissue[1]. Under such non-healthy conditions, elastin gene expression is down-regulated, and the mature elastin is degraded by MMPs and macrophage-derived elastases (cytokines, interleukins) into soluble peptides, which

furthermore interrupts elastin-SMC signaling pathways[18–23]. Such elastin disruption encourages SMC hyper-proliferation and medial thickening, leading to reduced arterial compliance, hypertension and aneurysm of the vessel[24–29]. The ability for vascular tissues to self-repair is hampered by their inherently complex matrix structure and compromised cell-signaling pathways.

The development of aneurysms might be one of the most prevalent cardiovascular conditions, possibly affecting up to 90% of people[30]. Due to the possibility of living with an aneurysm without it rupturing, as well as poor diagnosing methods, many conditions go untreated creating for an even larger risk. Besides, understanding the mechanisms leading to hypertension remain broadly unidentified[31]. As explained previously, the mechanical properties of cardiac tissue are obtained from the ECM, mainly the elastin and collagen fibers[32]. Since elastin functions mainly at lower pressures than collagen, the hypertension of vessel walls can be accounted for the degeneration of elastin, leading to many cardiac diseases[31].

Abdominal aortic aneurysms (AAA) is the extension of an abdominal aortic section, usually developing over several years, and is currently the 10th leading cause of death in the United States, killing roughly 15,000 people annually[33]. As stated previously, many of these cases are left undiagnosed and untreated, which results in a high mortality rate ~75-90%[34]. Many of the cases discovered are done so by accident during routine physical or radiographic exams on an unrelated symptom[34] and only six countries in the world offer a clinical screening procedure standard[35]. Other than the risk of rupture, the disruption of flow in the aneurysmal blood vessel can cause a multitude of symptoms depending on the type and location of the aneurysm, including; headaches, blurred or

double vision, weakness or numbness. The disruption of flow has been shown to change its direction to an anterior pathway moving along the proximal wall of the aneurysm creating a vortex[36].

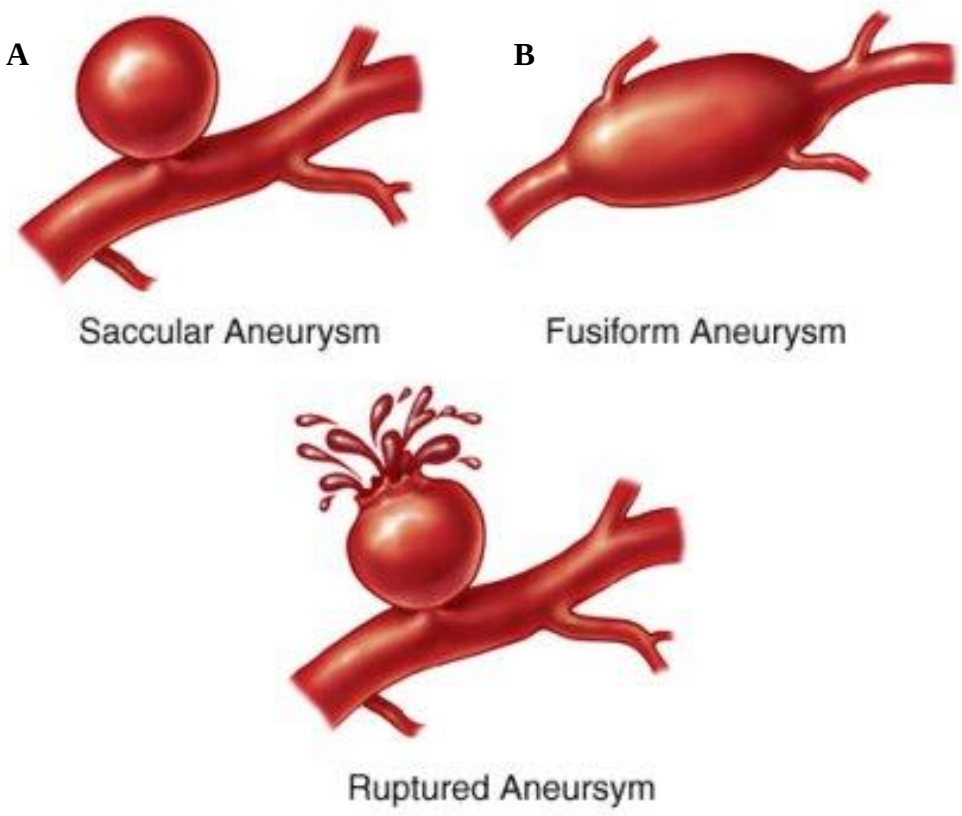

Figure 1.2 Different types of aneurysm formations (A) saccular and (B) fusiform[17].

1.4. Approaches for aneurysm treatment

As mentioned previously, early diagnosis of an aneurysm rarely occurs due to the lack of symptoms paired with the fact that many symptoms are not exclusive to aneurysms. The lack of early detection can lead to rupture of the aneurysm and depending on the severity of the hemorrhage death may result. The discovery a throbbing mass or the abnormal sound of rushing blood flow during a routine physical examinations can lead to further procedures including ultrasound, computed tomography

scan (CT), magnetic resonance imaging (MRI), or an angiography which will properly show the size and location of the aneurysm. Following the diagnosis of an aneurysm doctors will determine if surgical, pharmacological, or a mixture of both is best for the treatment. Treatment can also be in the form of altering patient behavioral factors which include the elimination of stressful situations, physical labor, smoking and unhealthy foods.

1.4.1. Surgical and Pharmaceutical approaches for aneurysm treatment

As described in the *History of Aneurysms* by W. E. Stehbens, treatment of aneurysms dates all the way back to the fourteenth century B.C. to the time of the Egyptians[37]. Treatment of aneurysms was first noted in 1817, when William and John Hunter performed the first ligation of an aneurysm[38]. The procedures evolved when the revolutionary surgical technique of endoaneurysmorrhaphy was developed in 1888 by Rudolf Matas[39]. In endoaneurysmorrhaphy the aneurysm is opened and then collapsed on itself through a series of folding to return the lumen of the blood vessel to is normal size and then sutured back together.

In the 1940's, advances in the treatment of congenital heart surgery lead to many of the modern surgical treatments of aneurysms. Here a ruptured aneurysm was first patched successfully utilizing a pectoralis muscle patch by Dr. Denton Cooley and Grant Ward[40]. This experience was vital for Dr. Cooley (along with Dr. Michael DeBakey) as he would later develop the tangential excision and lateral aortorrhaphy, which is the clamping of a saccular aneurysm at its neck and then removing the ballooned portion of

the artery[41]. Following their innovative treatment method Dr. Cooley and DeBakey were able to refine and apply the use of homografts in many new areas[41–47].

The next chapter of surgical treatments for aneurysms was started by Dr. Cooley in 1963 when he founded the Texas Heart Institute[40]. The Texas Heart Institute has decreased surgical mortality from 50% to 10% by modifying the Bentall and Cabrol procedure as well as perfecting bypass surgeries[48,49]. Lastly in 1981, Dr. Cooley innovative thinking led to the preparation of woven Dacron grafts, which he helped develop in 1978[50], by soaking them in the patient's own plasma and then autoclaved it which sealed the interstices of the graft with the coagulated protein. By doing this Dr. Cooley was able to reduce the post-surgery bleeding as well as start a standard for manufacturing of grafts today[49,51].

Besides open surgery techniques as described above, some aneurysms are able to be treated through a minimally invasive endovascular method. Two of the most common are stent graft repair and coil filling systems[52,53]. Both of these methods access the cardiovascular systems from a peripheral artery, and the most widely used in clinical settings currently. In the stent method the stent is put into place by a catheter and when in place, expands which allows blood to safely flow through and prevent any further damage to the aneurysm. As for the coil systems, they are utilized predominately in saccular aneurysms located in the brain due to the difficulty in performing open surgery. Similar to the stent, coil systems are loaded into a catheter and directed to the aneurysm site where they are deployed successfully filling up the ballooned area and sealing it from the artery.

In conjunction to surgical treatment route, pharmaceutical options are available. Medications (statins) can be used to combat a patient's high level of cholesterol which leads to an increase risk in atherosclerosis (a leading cause of aneurysms). Statins can block the enzymes necessary for the production of cholesterol, thus reducing the levels of cholesterol in the blood. Other drugs such as fibric acid derivatives, bile acid sequestrates, or nicotinic acid can also be used to control the cholesterol levels in the blood[54]. For treatment in patients already diagnosed with an aneurysm, beta-blockers are commonly prescribed as they can lower heart rate, and consequently the volume of blood pumped which ultimately lowers the blood pressure[55].

1.5. Tissue engineering approaches for aneurysm treatment

Tissue engineering is one avenue which within the last decade has made major strides in alleviating and identifying vascular aneurysms. Specifically improved biocompatibility of graft materials as well as cell delivery techniques for repair and regeneration of many cardiac diseases are one of several advances within the field that may one day lead to total vascular replacement; however these types of vascular conduits are limited by their dimensions, composition, and host response. The first tissue engineered vessel was created in 1986 by Weinberg and Bell[56] when they cultured bovine endothelial cells with smooth muscle cells and fibroblast in artificial blood vessels that had multiple layers of collagen and a Dacron mesh[57]. Culturing of the smooth muscle cells and fibroblast in the presence of vitamin C created an extracellular matrix that mimicked nearly to the *in vivo* characteristics[58]. Recently, several groups have attempted to utilize are ePTFE, Dacron, and polyurethanes for total vascular replacement but have

been unable to fully overcome host immune reaction[59]. Minimization of this immunogenic response can be achieved through surface treatment of the material using proteins, cells, and other polymers[60–62] which control the formation of thrombosis as well as hyperplasia within implanted grafts. Still the porous nature of these constructs allows for the diffusion of certain element into surrounding tissue. Lastly, Cambell et al. showed that when silastic tubing was inserted into the peritoneal cavity of rats and rabbits that it would cover the tubes with layers of myofibroblasts, a collagen matrix as well as a monolayer of mesothelial cells due to the inflammatory reaction. Once removed and turned inside out, the structure of the vessel mirrored that of normal tissue[63].

Another approach beside synthetic constructs is the use of acellular extracellular scaffolds formed from dehydrated mammalian tissue which can then be wrapped around a cylindrical mandril which gives it a tubular shape. Smooth muscle cells obtained from stem sources (embryonic, umbilical, and mesenchymal) can then be inserted into these lumens to form the vascular media. Finally after a week in a bioreactor or other growth stimulating conditions, these types of scaffolds can be implanted into host tissue and tested for viability[57]. Similarly, other groups have utilized a pulsatile flow in their scaffold design to help mature the tissues of their artificially constructed graphs to aid in their mechanical properties, specifically increased smooth muscle cell density, collagen density. One group reported on the addition of aortic smooth muscle cells placed in a silicone tube for 8 weeks with media pumped through at 165 beats per minute and 5% radial expansion[64]. In general, total vascular replacement is a promising option for those diagnosed with aneurysms; however currently due to the infancy of the field these approaches are not yet suitable for human trials.

1.6. Role of nitric oxide

Nitric oxide (NO) is an important signaling molecule that has a wide array of biological applications. NO is a small and relatively stable free-radical gas that readily diffuses into cells and interacts with molecular targets[65]. For the purpose of this thesis the studies of nitric oxide in cardiac tissue have been reviewed and their overall findings and scope of the experiments performed are mentioned in this section.

As discovered by Moncada et al., NO is synthesized from L-arginine substrate[66] and inhibited by N^G-monomethyl-L-arginine[67]. This group also discovered that the NO pathway existed in multiple tissues showing that NO is used in a wide range of cellular functions and communication[68–70]. They also claim that NO is an important regulator in blood pressure, platelet activation, as well as neurotransmission[71,72].

The work on the effects of NO on matrix synthesis ability by human vascular cells is lacking, but there has been work reported on vascular cells in other organisms. For example the administration of NO substrate was shown to suppress the induced pulmonary vascular disease in rats as well as $eNOS^+$ mice that exhibited increased pulmonary hypertension and vascular disease caused by chronic hypoxia[72,73]. This study shows that in rats that were treated with NO inhalation both reduced pulmonary vascular resistance as well as artery pressure by successfully dilating pulmonary vascular tissue. This shows that in the absence of NO leads to vasoconstriction and hypertension leading to many vascular diseases[73] as well as a decreased inflammatory response[72]. A similar study utilizing chick aortic SMCs show that the delivery of NO inhibits the proliferation of the cells and stimulates the expression of tropoelastin and LOX mRNA[74]. These studies give enough support to the possibility of utilizing exogenously delivered NO to

activate SMCs enzyme release, upregulate elastin synthesis and crosslinking through LOX upregulation, and return to normal homeostasis in diseased tissues.

The experiments described in this thesis utilize S-Nitrosoglutathione (GSNO) as a NO donor (**Fig. 1.3**). It has been previously found that the formation and decay of low molecular weight S- nitrosothiols (such as GSNO) may represent a mechanism for the storage or transport of NO[75,76]. Besides GSNO, other S-nitrosothiols include S-nitrosocysteine (CySNO) and S-nitroso-N-acetyl-DL-penicillamine (SNAP). GSNO is a preferred choice because it can be naturally occurring within the cell cytoplasm, has a low molecular weight of 336.32 (which allows for rapid diffusion across a scaffold), and possesses many different documented benefits to smooth muscle tissue such as protection against ischemic myocardium by increasing perfusion[77]. The decomposition of the S-nitrosothiols, mainly the hemolytic cleavage of the S-N bond[78], leads to NO release and thiyl radicals (GSH)[79]. It is also important to mention that the formation of S-nitrosothiols from endogenous NO intermediates readily reacts with glutathione to form naturally occurring GSNO[80,81]. Singh et al. showed that NO cleavage from GSNO readily occurs in the presence of light as well as transition metal ions. This group also claims that there is a transfer of NO^+ from an S-nitrosothiol to a thiol[79], this occurs through the presence of nicotinamide adenine dinucleotide phosphate-oxidase (NADPH oxidizing substrate) and thioredoxin reductases *in vivo*[82]. It could be postulated that the combination of metal ion chelators, specifically Cu^{2+} found in human smooth muscle cell cultures, along with additional cleavage occurring within the cell cytoplasm through the NADPH oxidizing substrate provides the necessary mechanism behind NO cleavage from GSNO molecules. For instance Singh et al. showed that GSNO released roughly 3/4^{ths} of

its NO within 30 minutes and over 600 μM of NO from 1 mM GSNO in the presence of Cu^{2+}[79].

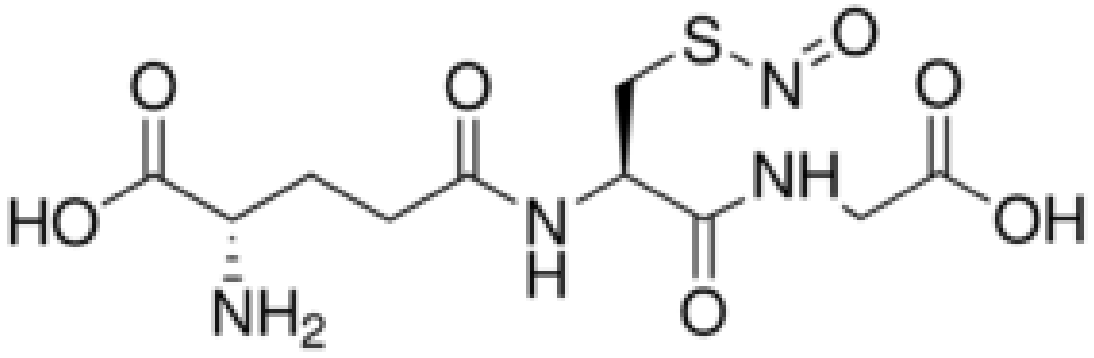

Figure 1.3 Chemical structure of S-Nitrosoglutathione[83]

Within physiological systems NO has many different functions in redox signaling[84–87]. Specifically, NO targets thiols that are specifically S-nitrosylated. The nitrosylation of a Cys-residue in $p21^{ras}$ activates the G protein, which plays a critical role in converting extracellular signals into intracellular biochemical events. Finally, the oxidation of NO *in vivo* has been proven to be very slow and insignificant process making it a relatively stable structure in the absence of glutathione which creates endogenous GSNO[88].

1.7. Organization of thesis

Data obtained in this thesis was organized into two separate experiments with the goal to describe the effects of delivering nitric oxide cues on HA-SMC proliferation, synthesis and deposition of vascular ECM (elastin, glycosaminoglycans, hyaluronic acid), release of inflammatory markers (MMPs-2, 9) and their inhibitors (TIMP-1), as well as matrix crosslinking enzymes (LOX). The first of these experiments utilized cocultures of HA-SMC and HA-EC. This was accomplished in both in a 3D microfluidic platform as well as 3D culture wells. The innovative microfluidic design allowed for paracrine

signaling as well as more physiologically relevant imaging while the culture wells allowed for quantitative analysis of the effects of both NO cues as well as HA-ECs on HA-SMCs. The second experiment was designed to utilize the key data obtained in the first and applied to diseased HA-SMCs with the exception of coculturing platform. Unlike the first experiment, culture wells were utilized in both 2D and 3D in order to properly translate data obtained in this thesis to future clinical relevance. This thesis was designed to obtain a thorough understanding of the exogenously delivered NO on both healthy as well as diseased HA-SMCs to be relevant for drug and toxicology screening, tissue engineering and regenerative medicine therapies, as well as vascular disease remodeling.

CHAPTER II

MATERIALS AND METHODS

2.1. Microfluidic platform fabrication

Coculturing vascular cells within 3D scaffolds, in close proximity to enable paracrine signaling, is difficult to accomplish using conventional cell culture techniques. This might partially explain the paucity of literature on this subject. Recent developments in microfluidic platforms might help overcome these limitations. The microfluidic device utilized in this study was created using photolithography and soft-lithography techniques as we detailed earlier[89]. Briefly, the device was designed in SolidWorks (SolidWorks Corp., Waltham, MA) and the mold developed at Stanford Microfluidics Foundry. Using this mold, microfluidic devices (**Fig. 2.1**) were created by replica molding with polydimethylsiloxane (PDMS: Dow Corning). PDMS was mixed with curing agent (10:1 ratio), degassed and cured, removed from the mold and cut into separate devices. The devices were then sterilized in boiling water (45 min), and dried (80 °C, 2 h). The glass

cover slips were cleaned with ethanol and air plasma treated along with PDMS devices for 1 min before bonding, and devices stored till usage in a sterile environment.

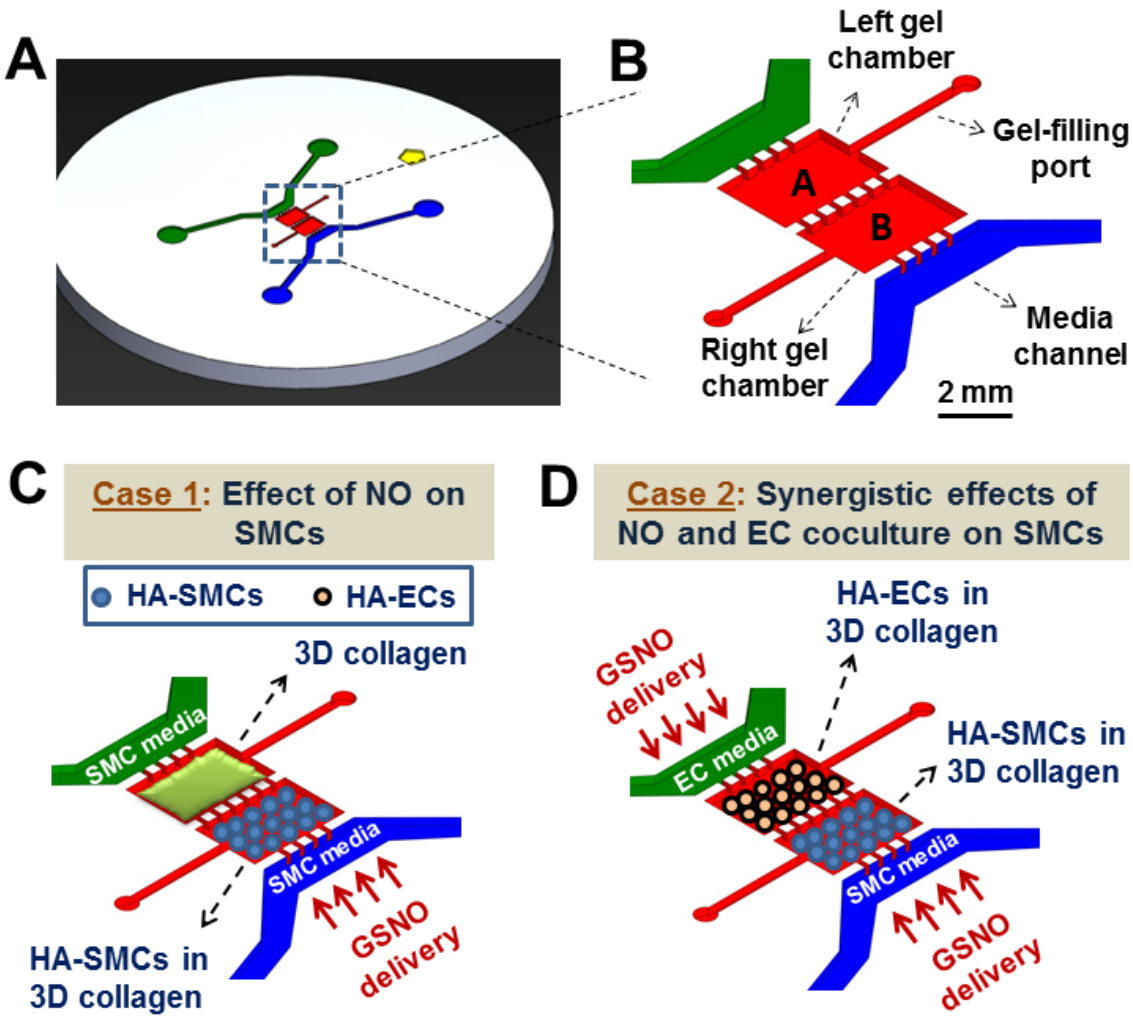

E

Case	Culture conditions		GSNO dose
	Chamber A	Chamber B	
1	*No cells*	*HA-SMCs*	0 - 100 nM
2	*HA-ECs*	*HA-SMCs*	0 - 100 nM

Figure 2.1 (A) Design of the microfluidic device for enabling biomimetic cocultures. (B) Cells could be cultured either alone or in the presence of other cell types within designated chambers of the device. These cell chambers have individual gel-filling ports, separated by microfluidic pillar posts, and could be supplemented with media through

separate channels. (C-E) HA-SMCs were cultured within collagen scaffolds, in the presence or absence of EC coculture and exogenous GSNO (0-100 nM dosage).

2.2. Cell culture

Healthy adult human aortic smooth muscle cells (HA-SMCs) and human aortic endothelial cells (HA-ECs) were obtained from Life Technologies Corp. (Carlsbad, CA) and passaged using appropriate media (Medium 231 and Medium 200, respectively; Life Technologies) provided. Diseased adult human aortic smooth muscle cells (HA-SMCs) were isolated from abdominal aortic aneurysm segment of a 54-year old male, and provided at passage 2 by collaborators at INSERM U698, Paris, France. These cells were passaged in our lab using appropriated media (Medium 231; Life Technologies). For experiments in this study, we used cells from passages 3-5 for healthy cells and 2-3 for diseased cells. Collagen gel (2 mg/ml; pH ~ 7.4) was prepared by mixing collagen stock solution (type-1, rat-tail derived, BD Biosciences, Bedford, MA) with a mixture of 10× PBS, 1 M NaOH and DI water.

2.2.1 Healthy cell cultures

Two sets of cultures were performed in parallel: (i) HA-SMCs cultured alone, and (ii) HA-SMCs co-cultured with HA-ECs both in a well as well as a microfluidic platform. Results from the former set serves to (a) establish baseline data for adult human aortic SMC 3D cultures, (b) act as a control for the adult vascular 3D coculture data, and (c) rapidly scale up this process for further *in vitro* or *in vivo* studies. SMCs or ECs were mixed in 2 mg/ml collagen at a density of 10,000 cells per chamber. The device has two separate but adjacent 3D chambers (**Fig. 2.1**), each with individual gel-loading ports and

media channels. As shown in **Fig. 2.1**, in devices where SMCs were cultured alone, collagen gel containing SMCs were injected in the right chamber of the device, and collagen gel containing no cells in the left chamber. Similarly, in cases where cocultures were performed (**Fig. 2.1**), collagen gel containing ECs were injected in the left chamber, and gel containing SMCs in the right chamber. In this fashion, each cell type received its own media and GSNO dosage, but still in constant diffusive contact with neighboring cell type. Gels were injected into the respective gel-loading chambers with a cold-pipette tip containing ~7 µl of collagen solution. The devices were placed in a humidified incubator (37 °C, 30 min) to polymerize the collagen. Upon polymerization, cells were cultured for 21 days in either SMC or EC media, containing S-Nitrosoglutathione (GSNO; Sigma, Saint-Louis, MO), an NO donor.

As detailed in **Fig. 2.1** (cases 1 and 2), four different concentrations of GSNO (0, 1, 10, 100 nM) were tested for their ability to induce changes in SMC proliferation and matrix synthesis. GSNO concentration at 0 nM acts as a control for higher GSNO concentrations in each case. We choose not to coculture HA-SMCs with HA-SMCs (in separate chambers), due to minimum benefits from autocrine signaling. These devices could be scaled up in dimensions, for culturing larger gel volumes or higher cell densities. As for the well culture platform 300 µl of collagen gel containing 10,000 cells was seeded into a 48-well plate. Plates were placed in the humidified incubator (37 °C, 30 min) to polymerize the collagen and then cultured for 21 days in a similar method to the microfluidic device. The main difference was that in the case of coculture the HA-EC spent media was transferred to the HA-SMC cultures. Media was changed once a day and the spent medium was pooled over the 21 day culture and stored at -20 °C for further

biochemical analyses. Similarly, cell matrix layers at the end of 21 days were trypsinized (one chamber at a time) and pooled from respective chambers and processed for biochemical assays as detailed below.

2.2.1 Diseased cell culture

Two sets of cultures were performed in parallel: (i) Aneurysmal HA-SMCs cultured on 2D substrates, and (ii) HA-SMCs cultured within 3D collagen hydrogels. To seed the wells in 3D cultures, SMCs were mixed in 2 mg/ml collagen at a density of 10,000 cells per well, while in 2D seeding the 24-well plates were first coated with a layer of 50 µg/ml collagen and then 10,000 cell were placed in each well. The cultures were placed in a humidified incubator (37 °C, 30 min) to polymerize the collagen. Upon polymerization, cells were cultured for 21 days in SMC media, containing S-Nitrosoglutathione (GSNO; Sigma, Saint-Louis, MO), an NO donor. Two different concentrations of GSNO (0 and 100 nM) were tested for their ability to induce changes in SMC proliferation and matrix synthesis, based on outcomes identified in healthy cell cultures. A total of 12 wells were seeded for both 2D and 3D cultures per concentration of GSNO. GSNO concentration at 0 nM acts as a control for higher GSNO concentrations in each case. Media was changed once a day and the spent medium was pooled into a single volume per case over the 21 day culture and stored at -20 °C for further biochemical analyses. Similarly, cell matrix layers at the end of 21 days were trypsinized (one chamber at a time) and pooled from respective chambers and processed for biochemical assays as detailed below.

2.3. Biochemical analyses

The characterization of the ECM synthesized by both the healthy and diseased HA-SMCs was performed by the assays as described in the sections below. For each of these assays there were conducted on both the cell matrix as well as the pooled media (1 case per assay with n=3 per case unless otherwise noted) following the 21 day culturing period. For healthy cell cultures, cells were seeded within one well per assay due to extremely low proliferation rate of adult HA-SMCs, low survival after passaging, and the prohibitive costs in obtaining large cell densities required for seeding in larger number of wells . To prepare each sample for their respective assay the cell matrices were detached by incubating them with Trypsin 1× for 8-10 min. Once the cells were detached from each well the suspensions were centrifuged at 2800-3000 rpm for 10-12 min. Following the centrifugation, the supernatant was discarded leaving the pellet in the microcentrifuge tube. The pellet were resuspended in 300 µL of 1x PBS. Similarly the pooled media that was collected from each well and stored at -20 °C, was thawed and distributed in 1 mL increments to labeled microcentrifuge tubes and centrifuged at 12000 rpm for 15 min. Once the centrifuging was complete the supernatant was discarded and the pellet was resuspended in 300 µl of 1x PBS. All samples were then stored in -20 °C until further use. Before the start of any assay the samples were thawed at room temperature.

2.3.1. DNA assay for cell proliferation

The cell density within different cases was quantified at the end of both 1 and 21 days to assess the proliferation of healthy or diseased HA-SMCs and HA-ECs over the culture period. Briefly, media was removed from the media channels, and 0.25% v/v trypsin-

EDTA (Invitrogen) was added to the channels, cell layers were detached and extracted separately from each chamber, pelleted by centrifugation, resuspended in NaCl/Pi buffer, and assayed using a fluorometric assay, as we detailed earlier[89]. The cell density was calculated on the basis of an estimated 6 pg DNA/cell[90].

2.3.2. BCA assay for total protein synthesis

The total amount of protein synthesized by HA-SMCs under various culture conditions was determined using bicinchoninic acid protein assay kit (BCA Kit, Sigma-Aldrich), as per the vendor's protocols. Once thawed 25 µl of each sample were pipetted into a 96-well plate (Greiner Bio One, Monroe, NC) along with the standards that were prepared according to the venders protocol of 25 µg/ml, 125 µg/ml, 250 µg/ml, 500 µg/ml, 750 µg/ml, 1000 µg/ml, 1500 µg/ml, and 2000 µg/ml. To each of the wells containing either a sample or a standard 200 µl of BCA working solution was added and mixed on a mechanical shaker for 30 seconds. This assay is based on the principle that a Cu^{2+}-protein complex forms under alkaline conditions, followed by reduction of the Cu^{2+} to Cu^{1+} based on the amount of protein present in the sample and has a working range of 20-2000 µg/mL (all data obtained was within this range). The total protein in the pooled spent media as well as in the cell matrix at the end of 21 days was quantified (n = 6 devices/condition).

2.3.3. Fastin assay for elastin protein

The amounts of matrix elastin and tropoelastin (in pooled spent medium) were quantified using a Fastin assay (Accurate Scientific Corp, Westbury, NY, USA). Since

the Fastin assay quantifies only soluble α-elastin, the matrix elastin was first reduced to a soluble form and has a working range of 5-70 µg (all data was found within this range and n=4 for healthy monocultures and cocultures). This was accomplished by digesting the samples with 1 M oxalic acid at 100 °C for one hour. The samples were then transferred to a 2 ml microcentrifuge tube and with an equal amount of elastin precipitating reagent. Along with this step the elastin precipitating reagent was also added to the blanks and standards (12.5 µl, 25 µl, and 50 µl). It is important to note that both samples and standards were run in duplicate in accordance to the Fastin elastin assay protocol. Once the elastin precipitating reagent was added to all samples and standards each tube was vortexed and left at room temperature for 15 minutes. Following the 15 minutes the tubes were centrifuged at 10,000 g for 10 minutes and following the supernatant was removed. The pellet containing the elastin precipitate was suspended in 1 ml dye reagent and homogeneously mixed on a mechanical mixer at room temperature for 90 minutes. Following incubation, each tube was centrifuged as described above and 250 µl Dye dissociation reagent was added to each tube once the supernatant was removed. The pellet was then dispersed by vortexing twice with a 10 minute interval. The suspension was then transferred to a 96-well microplate and the absorbance was measured at 513 nm with a microplate spectrophotometer. The measured amounts of matrix elastin and tropoelastin were normalized to their respective cell counts to provide a reliable basis of comparison between samples.

2.3.4. sGAG assay for glycosaminoglycan synthesis

The amounts of sulfated glycosaminoglycans deposited within the cellular matrix as well as in the pooled spent medium were quantified using a quantitative dye-biding sGAG Assay (Kamiya Biomedical Company, Seattle, WA) as per vendor's protocols. A volume of 50 µl in duplicated of standards, blanks, controls, and samples were diluted with 50 µl of 8M Guanidine-HCL and incubated for 15 minutes at room temperature. 50 µl of 0.3% (GuHCl) and incubated for 15 min at RT. A diluent composed of 0.3% H2SO4 and 0.75% Triton X-100 was added to each vial and mixed at room temperature for 15 minutes on a mechanical mixer. Once mixed, 750 µl of Alcian blue working solution was added to each vial. To allow the Alcian blue to bind to the sGAG the vials were incubated overnight at 4°C. The following day the vials were centrifuged at 12000 for 15 minutes. The supernatant was then removed and the pellet was resuspended in 500 µl DMSO solution and mixed for 15 minutes at room temperature. Following the mixing, the vials were then centrifuged again as previously with the supernatant being discarded and 500 µl of Gu-Prop (4M GuHCl + 33% 1-propanol + 0.25% Triton X-100) was added. Once the pellet was dissolved the samples were loaded onto a 96-well plate and the absorbance values were read at 620 nm on an Epoch™ microplate spectrophotometer (Bio-Tek, Winooski, VT), and the measured sGAG amounts were normalized to the corresponding cell counts (n = 6 devices/condition for the healthy monoculture and cocultures). This assay is based on the specific interactions between sulfated GAGs and the tetravalent cationic dye Alcian blue, at low pH and optimized ionic strength and has a working range of 12.5-400 µg/mL. Most data points were not within this range increasing the amount of error. To obtain results a smaller standard

curve was calculated using the low standards which allowed for the calculation of GAG molecules in the lower ranges. It should be noted that this assay will not quantify the non-sulfated GAGs such as hyaluronic acid.

2.3.5. HA assay for hyaluronic acid synthesis

Hyaluronic acid synthesized and released by SMCs within the cellular matrix as well as in the pooled spent medium was quantified using a hyaluronan enzyme-linked immunosorbent quantitative assay (Echelon Biosciences Inc., Salt Lake City, UT). HA concentration in the sample is determined using a standard curve of known HA amounts. This assay works best with HA molecules that are greater than 25 repeating units. Because this assay has a working limit depending on the number of repeating units it is difficult in the scope of this study to ensure the presence of any HA molecules that are shorter than 25 repeating units. A volume of 100 µl samples and standards were pipetted in the provided 96-well incubation plate. To act as the zero HA control in this assay 100 µl of 1x HA diluent was utilized while for the blank control 150 µl of the diluent was used. 50 µl of the diluted HA working detector was added to each of the wells except for the ones filled with the blank controls. Following the addition of the diluted HA working detector the plate was gently mixed and incubated for one hour at 37 °C. Once the incubation period was complete 100 µl of the solution was transferred from each well to the corresponding well in the pre-coated HA detection plate. The detection plate was then incubated for 30 minutes at 4 °C and then each well was washed four times with 1x wash concentrate making sure to invert and remove all wash concentrate onto an absorbent paper towel. After the washing step was complete 100 µl of working enzyme

was added to each well and incubated for 30 minutes at 37 °c. The washing procedure described above was repeated following the incubation and 100 µl of working substrate solution was added to each well. The detection plate was then incubated in the absence of light at room temperature for 15 minutes and the absorbance was measured. Absorbance values were read at 450 nm on an Epoch^{TM} spectrophotometer every 15 minutes until the ratio between the zero HA control and the 1600 ng/ml HA standard is higher than 3. This ratio indicates the completion of the reaction and to add the stop solution to each well. The measured HA content was normalized to the corresponding cell counts (n = 6 devices/condition).

2.3.6. LOX functional activity

Studies have shown that lysyl oxidase (LOX) and LOX-like proteins are endogenous enzymes responsible for crosslinking elastin precursor (tropoelastin) molecules. Thus, estimating the endogenous LOX activity in the cellular matrix as well as in pooled medium indicates the extent of cell-mediated crosslinking of tropoelastin to form mature elastin matrix structures. Using a fluorometric assay (AmplexRed® Assay; Molecular Probes, Eugene, OR), we assayed for LOX activity within the cell matrix and pooled spent culture medium aliquots from different culture conditions. This assay works on the principle that H_2O_2 will be released when LOX oxidatively deaminates alkyl monoamines and diamines and has been used to detect as little as 10 pM of H_2O_2 in a 100µL volume (all measured values are above this detection limit). Firstly, the standards were prepared (0, 2, 4, 6, 8, and 10 µM) and 50 µl of each standard and samples were pipetted into a 96-well microplate with 50 µ of working solution (100µM Amplex Red

reagent, 1:2, 0.2 U/ml Horseradish peroxidase). The microplate was then incubated in the dark for 30 minutes at room temperature. Fluorescence intensities were recorded with excitation and emission wavelengths of 560 and 590 nm, respectively (560 nm gave the best standard curve and thus was used). The measured activity was normalized to the cell density within that respective culture condition (n = 3 devices/condition).

2.3.7. Quantification of MMPs-2, 9 and TIMP-1 release

The amounts of MMPs-2 and 9 deposited within the cellular matrix as well as in the pooled spent medium were quantified using MMP-2 ELISA (Boster Biological Technology Co., Fremont, CA) and MMP-9 ELISA (R&D Systems, Inc., Minneapolis, MN) assays as per vendor's recommendations. The amount of TIMP-1 deposited within the cellular matrix as well as in the pooled medium was quantified using a TIMP-1 ELISA (Boster Biological Technology Co.). The measured MMPs and TIMP-1 content was normalized to the respective cell count within those cultures (n = 6 devices/condition). For the MMP-2 ELISA the sensitivity is < 10 pg/mL, MMP-9 ELISA is <13 pg/mL, and TIMP-1 ELISA is < 3 pg/mL. Samples studied from the cell matrix showed insignificant amounts of MMPs and TIMPs making it hard to accurately quantify the actual amount of each protein however samples obtained from the pooled media all showed values larger than the working limit.

2.3.7.1 Quantification of MMPs-2 and TIMP-1

The same provided protocol procedure was followed for both the MMPs-2 and TIMP-1 assays. Firstly, each sample was diluted 2:1 with the provided diluent buffer and then

100 µl of each sample was pipetted in the corresponding MMP-2 and TIMP-1 specific antibody pre-coated 96-well plate. Following, 100 µl of the respective standards were then pipetted into the respective plates. The microplates were then covered and incubated at 37 °C for 90 minutes. Ensuing the incubation, each plate was carefully blotted on an absorbent paper allowing the wells to dry and then the plates were incubated for one hour at 37 °C with 100 µl biotinylated anti-rat MMP-2 and TIMP-1 antibody working solutions added to their respective wells. Next, the solution was discarded from each microplate and each well was then washed three times with 1x PBS. Following the washing step, the plates were incubated with 100µl of 1x Avidin-Biotin-Peroxidase Complex for 30 minutes at room temperature. The solution was then discarded and the wells were washed five times with 1x PBS. 90 µl TBM color developing agent was then added to each well and the plates were incubated at 37 °C for 30 minutes before the reaction was terminated with 100 µl of TMB stop solution in each well. The absorbance was read at 450 nm.

2.3.7.2 Quantification of MMPs-9

The MMP-9 ELISA assay is based on the quantitative enzyme-linked immunoassay method where the MMP-9 binds to a specific monoclonal antibody and a specific enzyme-linked polyclonal antibody. 50 µl of diluent RD1-34 was pipetted to each well in the provided pre –coated 96-well plate with 50 µl of standards and samples. Once these two were added the plate was then covered and incubated for two hours at room temperature. Following the incubation, the wells were washed with wash buffer five times and 100 µl of MMP-9 conjugate was added to each well. The incubation and

washing step were repeated and then 100µl of substrate solution was added to each well. Following the addition of the substrate solution the plate was incubated in dark at room temperature for 30 minutes. Lastly, 100 µl of stop solution was added to each well and the absorbance was measured at 450 nm and 570 nm. To obtain the standard curve and thus the MMP-9 content the absorbance read at 570 nm was subtracted from 450 nm.

2.4. Immunofluorescence imaging of matrix proteins

The presence of elastin, fibrillin and LOX proteins within cell matrix were qualitatively confirmed using immunofluorescence labeling (n = 3 devices/condition for each protein). The presence of fibrillin within cell layers will confirm whether elastin matrix formation was mediated by pre-deposition of a fibrillin scaffold. At 21 days, the cell layers within microfluidic devices were fixed with 4% w/v paraformaldehyde for 15 min, and incubated with blocking serum (5% goat serum, 0.3% Triton-100 in phosphate-buffered saline; 20 min; 25 °C). Elastin, fibrillin and LOX were detected with respective polyclonal antibodies (1% antibody in 1X PBS, 5% goat serum, 0.1% Trition-X, Elastin Products; Abcam; Santa Cruz Biotechnology), which were incubated overnight at 4 °C on a mechanical shaker. Once incubation was complete each cell culture was washed 3 times with 1x PBS, allowing 5 minute intervals between washes and then appropriate secondary antibodies (0.4% antibody in 1x PBS, 5% goat serum, 0.1% Triton-X, Chemicon, Temecula, CA) were added and incubated at room temperature in the dark for 20 minutes. Cell nuclei were visualized with the nuclear stain 4', 6- diamino-2-phenylindole dihydrochloride (DAPI) contained in the mounting medium (Vectashield; Vector Labs, Burlingame, CA) and 1X PBS was added to preserve cell culture till

florescence imaging was performed. Images were acquired with a Zeiss Axiovert A1 florescence microscope equipped with Hamamatsu camera and image acquisition software. Please see **Table 2.1** for proper antibodies to be used in Immunofluorescence imaging.

Table 2.1 Summary of antibodies used in immunofluorescence analysis.

Primary Antibody	**Host**	**Clonality**	**Concentration (v/v)**
Elastin	Rabbit	Polyclonal	1;100
LOX	Rabbit	Polyclonal	1;100
Fibrillin	Rabbit	Polyclonal	1;100
Secondary Antibody	**Host**	**Clonality**	**Concentration (v/v)**
Goat anti-Rabbit	Goat	Poluclonal	1;250

2.5. Cellular Dimensions

The dimensions of the healthy and diseased phenotype were imaged using a Zeiss Axiovert A1 florescence microscope equipped with Hamamatsu camera and image acquisition software. Six cases per cell type were used and processed through ImageJ software where each perimeter and area was calculated. Each case was sampled during the 3-5 passages and seeded on a T-25 plate with Medium 231.

2.6. Statistical analysis

All biochemical data were obtained from three independent repeat experiments per case, and were analyzed using Student's t-test and one-way ANOVA, assuming unequal variance and differences deemed significant for $p < 0.05$. The data were assumed to

follow a near-Gaussian distribution in all the cases, and the mean and standard errors were calculated accordingly.

CHAPTER III

RESULTS AND DISCUSSION: HEALTHY HUMAN SMCS WITHIN COCULTURES

3.1. HA-EC and HA-SMC proliferation

The proliferation of HA-ECs and HA-SMCs cultured in the presence or absence of GSNO are shown in **Fig. 3.1**. In the absence of GSNO (controls), ECs proliferated ~ 3-fold over 21 days, compared to their original seeding density (**Fig. 3.1 A**). The addition of 1 or 10 nM GSNO promoted EC proliferation by ~4.1-fold and 4.8-fold respectively, compared to day 1 seeding ($p < 0.01$ vs. controls in both the cases). Addition of 100 nM GSNO offered no further benefit to EC proliferation compared to controls ($p = 0.2$ vs. controls). In the presence or absence of GSNO, trends in SMC proliferation rates were different from that of ECs. When SMCs were cultured alone in the absence of ECs, increasing GSNO concentration suppressed SMC proliferation within 3D collagen scaffolds over the 21 day period (**Fig. 3.1 B**). SMCs proliferated ~ 3.2-fold in the absence

of GSNO, and that reduced to 2.9-fold, 2.4-fold and 2-fold respectively, in the presence of 1, 10 and 100 nM GSNO ($p < 0.01$ for 0 nM vs. 10 nM or 100 nM; $p < 0.01$ for 1 nM vs. 100 nM). In the presence of EC cocultures, SMCs proliferated almost 4.8-fold and 3.9-fold respectively, at 0 nM and 1 nM GSNO concentrations ($p < 0.01$ for EC coculture vs. no coculture, under respective conditions; $p < 0.01$ for 0 nM vs. 1 nM GSNO). However, SMC proliferation rates significantly decreased to 2-fold and 1.4-fold, with the addition of 10 nM and 100 nM GSNO respectively, within cocultures ($p < 0.01$ for 10 nM vs. lower concentrations of GSNO; $p < 0.01$ for 100 nM vs. lower concentrations of GSNO; $p < 0.01$ for 10 nM vs. 100 nM GSNO).

Previous studies have shown that the half-life of GSNO ranges from 5.5 h to 24 h, depending on pH and environmental conditions[82,91], and is considerably higher than that of pure NO (typically a few minutes)[92]. Therefore, we choose to replace the culture medium twice a day, so that fresh NO is delivered to the cells within cultures. Besides, the NO release from GSNO concentrations tested here are within the physiological levels[92], which makes this study a good starting point for further *in vivo* optimization studies. Given that NO is an unstable gas and endogenous NO levels are impossible to quantify or manipulate, exogenous aerosolized NO delivery has been used to positively modulate circulating levels of NO within cystic fibrosis patients[93]. In this study, we did not investigate the NO activity and release rates from GSNO within culture media at neutral pH, as it has been extensively reported earlier[94,95]. Given the low molecular weight, it takes less than 20 min for GSNO (or NO) to diffuse across the 3D collagen scaffold within the microfluidic device and saturate the entire cell culture region.

Exogenously delivered NO has been shown to suppress proliferation of endothelial cells derived from fetal bovine aorta and human umbilical veins in a dose-dependent manner[96], via an intracellular cGMP mechanism. In contrast, we noticed here that lower GSNO dosage (1-10 nM) promoted modest HA-EC proliferation, while the stimulatory effect was attenuated at 100 nM GSNO. Our results on the dose-dependent inhibitory effects of GSNO on HA-SMC proliferation are in excellent agreement with similar studies evaluating the role of NO donors (e.g., DEA NONOate, sodium nitroprusside, nitroglycerin, SNAP) on human, rabbit, chick or rodent SMCs, both *in vitro* and *in vivo*[74,92,94,97]. It is worth mentioning that cell toxicity was not noted within our cultures (from LIVE/DEAD assay analysis; data not shown) in the presence of GSNO, and the cell morphology appeared identical in both controls and test cases. SMC proliferation data within cocultures was also in agreement with studies by Fillinger et al., who reported that within bovine aortic cell 2D cocultures, ECs stimulated SMC proliferation by ~56% compared to culturing SMCs alone[98]. Taken together, our results unequivocally suggest that vascular cell proliferation is differentially modulated by exogenous NO delivery, with significant implications in vascular remodeling under healthy and diseased conditions.

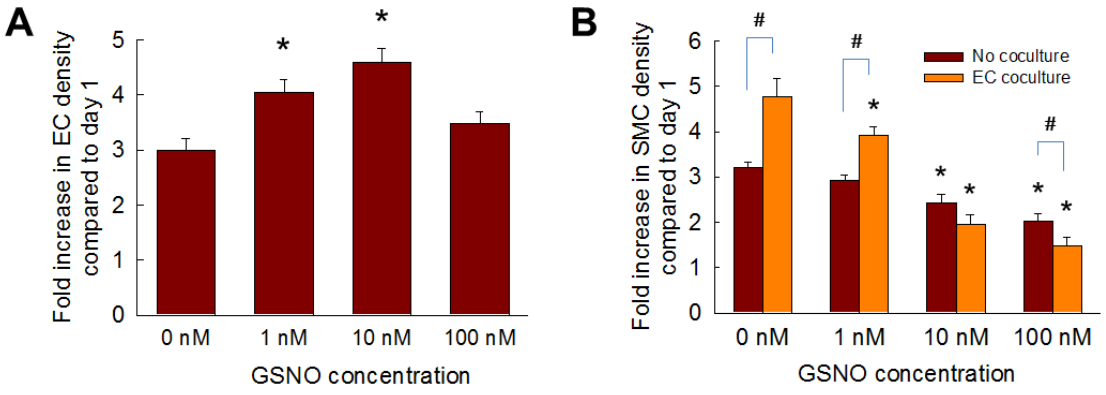

Figure 3.1 (A) Fold increase in HA-EC density within 3D cultures supplemented with

GSNO (0-100 nM). (B) Proliferation ratios of HA-SMCs in the presence or absence of EC cocultures and GSNO (0-100 nM). Data shown represent mean ± standard error of cell count after 21 days of culture, normalized to initial seeding density (n = 3/ condition). * indicates $p < 0.01$ compared to GSNO-free cultures; # indicates $p < 0.01$ for no cocultures vs. EC coculture, at a given GSNO dosage.

3.2. Total protein synthesis by HA-SMCs

The total protein amounts synthesized by HA-SMCs, in the presence or absence of ECs, were quantified as two separate components: released into pooled spent media and that deposited in cell matrix. HA-SMCs produced and deposited ~131 ± 19 ng of protein within cell matrices, on a per cell basis, when cultured alone in the absence of GSNO (**Fig. 3.2 A**). Although 1 and 100 nM GSNO offered no further benefits to protein deposition within these SMC cultures, 10 nM GSNO significantly suppressed protein deposition within SMC cultures (~ 67.8 ± 9 ng of protein; $p < 0.001$ for 10 nM vs. all the other cases). On the other hand, coculturing SMCs with ECs did not improve protein deposition in cell matrix in the absence of GSNO. Within EC cocultures, only 100 nM GSNO stimulated a 2.2-fold increase in total protein deposition within cell layers, compared to GSNO-free cultures ($p < 0.001$ for 100 nM vs. lower GSNO doses).

HA-SMCs released ~ 2 ± 0.15 µg of protein into pooled media on a per cell basis, over the 21 day culture, in the absence of EC cultures and GSNO (**Fig. 3.2 B**). While the addition of 1 nM and 10 nM GSNO did not alter these amounts, 100 nM GSNO upregulated protein release by 1.54-fold compared to non-additive controls ($p = 0.008$). Surprisingly, coculturing with ECs significantly suppressed protein release into pooled media by SMCs, on a per cell basis, compared to their stand-alone cultures (**Fig. 3.2 B**; $p < 0.001$ for no coculture vs. EC coculture controls). Addition of 1 nM GSNO did not rescue this decrease in protein synthesis and release by SMCs within cocultures.

However, 10 nM and 100 nM GSNO addition stimulated 1.42- and 3.66- fold increases in protein synthesis by SMCs within EC cocultures, compared to controls ($p = 0.026$ and $p < 0.001$, respectively, compared to controls). Taken together, results suggest that 100 nM GSNO dosage significantly increased total protein synthesis, release into pooled media and deposition within cell matrix layers, in the presence or absence of EC cocultures.

The effects of NO on matrix protein synthesis by SMCs or any other mammalian cell types has been reported in a very few studies thus far. Kolpakov et al. have shown that NO donors such as SNAP (0.4-1.2 mM) and SNP (0.1-0.5 mM) inhibited total protein synthesis and collagen synthesis by rabbit aortic SMCs *in vitro* in a reversible but dose-dependent manner[99], highlighting the strong role of NO in modulating SMC phenotype. In another study, SNAP inhibited total protein synthesis by rat aortic SMCs in a time-dependent manner, when cultured in the presence of 5% fetal calf serum[100]. Curran et al. have shown that SNAP inhibited total protein synthesis by hepatocytes in a reversible but dose-dependent manner[101]. These results are in agreement with our observations, where NO delivered via GSNO did not significantly enhance total protein synthesis by HA-SMCs, except at 100 nM dosage and EC coculture. Although the molecular mechanisms behind this NO-mediated inhibition of protein synthesis by SMCs remains categorically unexplored and beyond the scope of this work, previous studies suggest that multiple biochemical pathways might be involved in mediating this process[99].

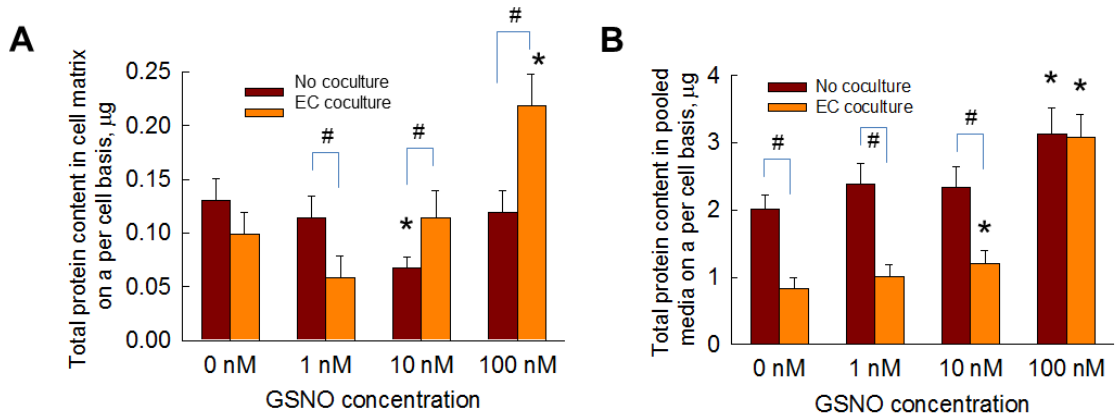

Figure 3.2 Total protein amounts deposited within cell matrix (A) or released into pooled media (B), when GSNO (0-100 nM) was supplemented to HA-SMC cultures, in the presence or absence of HA-EC cocultures. Data shown represent mean ± standard error of protein synthesis after 21 days of culture, normalized to cell count within respective cases (n = 6/ condition). * indicates $p < 0.05$ compared to GSNO-free cultures; # indicates $p < 0.01$ for no cocultures vs. EC coculture, at a given GSNO dosage.

3.3. Elastin synthesis and deposition by HA-SMCs

The total elastin synthesized by HA-SMCs was quantified as that released into pooled media (i.e., tropoelastin) and that deposited into the cell layers (i.e., matrix elastin). In the absence of EC coculture and GSNO, HA-SMCs released 7.05 ± 1.1 ng of tropoelastin on a per cell basis over the 21 day culture (**Fig. 3.3 A**). Within SMC cultures, the tropoelastin content increased to 11.8 ± 2.2, 42.3 ± 5.4 and 29.9 ± 4.7 ng respectively, in the addition of 1, 10 and 100 nM GSNO ($p < 0.01$ for 0 nM vs. higher GSNO dosages). Thus, in the absence of EC cocultures, 10 nM GSNO appeared to stimulate higher tropoelastin synthesis and release by HA-SMCs ($p < 0.01$ vs. all other GSNO dosages). Even in the absence of GSNO, coculturing with ECs stimulated significantly higher amounts of tropoelastin release by SMCs (**Fig. 3.3 A**; 20.6 ± 3.8 ng per cell) compared to that within no coculture cases ($p < 0.001$ for EC coculture vs. no coculture). Within cocultures, addition of 10 nM or 100 nM GSNO furthered tropoelastin synthesis by 2.4-

and 3.2- fold respectively, compared to that seen in controls ($p < 0.001$ for 0 nM vs. 10 nM or 100 nM GSNO). However, no significant benefit of cocultures to tropoelastin synthesis was noted at 1 nM GSNO dosage.

In the absence of EC cocultures, matrix elastin deposited within HA-SMC cultures was undetectable at 0 nM GSNO (**Fig. 3.3 B**). However, with increasing GSNO dosage, matrix elastin amounts on a per cell basis increased in a linear fashion, with significant differences noted between incremental GSNO dosages ($p < 0.01$ for 0 nM vs. 1 nM, 1 nM vs. 10 nM, and 10 nM vs. 100 nM). Even in the absence of GSNO, coculturing with ECs resulted in the deposition of 1.76 ± 0.25 ng of matrix elastin by SMCs, on a per cell basis. Within EC cocultures, addition of 1, 10 and 100 nM GSNO resulted in 1.2-, 2.9- and 4-fold increases in matrix elastin synthesis on a per cell basis, compared to GSNO-free controls ($p < 0.01$ for 10 nM vs. 0 nM, and for 100 nM vs. 0 nM). Taken together, results suggest that (a) although adult HA-SMCs produce quantifiable tropoelastin over the 21 day culture period, they do not deposit detectable amounts of matrix elastin, in the absence of GSNO; (b) coculturing with ECs significantly upregulated tropoelastin and matrix elastin by adult HA-SMCs, even in the absence of GSNO; (c) GSNO addition significantly enhanced both tropoelastin release and matrix elastin deposition by SMCs in a dose-dependent manner, in the presence or absence of EC cocultures; and (d) EC coculture and 100 nM GSNO synergistically contributed to multi-fold increases in tropo- and matrix elastin by adult HA-SMCs.

From the data shown in **Figs. 3.3 A** and **B**, the matrix elastin yield (ratio of matrix elastin to the total elastin produced) within these HA-SMC cultures was calculated. When SMCs were cultured alone in the absence of ECs, the matrix elastin yields were 5%, 2.3%

and 4.1% within 1 nM, 10 nM and 100 nM GSNO additive-cultures, respectively. However, EC cocultures significantly enhanced matrix elastin yields, both in the presence or absence of GSNO. The matrix elastin yield within 0 nM, 10 nM and 100 nM GSNO additive cultures were 7.8%, 9.3% and 9.8%, respectively ($p < 0.001$ for no coculture vs. EC coculture, at respective GSNO doses). Surprisingly, addition of 1 nM GSNO resulted in ~ 40% matrix elastin yield, significantly higher than that noticed in all the other coculture cases.

Despite recent progress in the field of vascular tissue engineering, elastin synthesis and deposition by vascular SMCs within 3D constructs remain a formidable challenge[102,103]. This is partially due to highly reduced ability of adult SMCs (at both transcription and translation levels) to synthesize, release, and deposit mature elastin. Thus, the overarching goal of cellular or tissue engineering approaches is to stimulate these adult SMCs, using an optimal combination of biochemical and biomechanical cues, to deposit mature and cross-linked elastin within blood vessels. In a series of studies, we have shown that exogenous cues such as hyaluronan oligomers, TGF-ß1, IGF-1 and LOX induced increases in elastin synthesis within 2D cultures of adult rat aortic SMCs[89,104–107]. In a series of recent studies, Lin et al. have shown that surface topography strongly affects elastin gene expression and protein synthesis by adult human coronary artery SMCs[108,109]. Elastin gene expression and protein synthesis by these cells increased significantly when cultured within 3D porous polyurethane scaffolds compared to their 2D culture counterparts, and the addition of TGF-ß1 to these cultures furthered these trends. Such increases in elastin expression by SMCs within these 3D scaffolds were facilitated by Ras-ERK1/2 signal transduction pathways. However, these cells were

cultured only up to 14 days, which is not sufficient for elastin matrix deposition and maturation within cell layers. Ramamurthi and coworkers recently showed that adult human and rat SMCs produced higher elastin protein within 3D collagen gels exposed to exogenous growth factors or cyclical stretching conditions[110,111]. These studies point to the overall superiority of 3D scaffolds over 2D cultures, in stimulating elastin synthesis and release by SMCs.

Thus, in this study, we cultured HA-SMCs within 3D collagen scaffolds to mimic physiological conditions, and enable future tissue engineering based approaches for in situ elastin regeneration. We noted multi-fold increases in tropoelastin production and matrix elastin deposition within HA-SMC 3D cultures, in the presence of GSNO and EC cocultures. A study by Sugitani *et al*. was the only known report which evaluated the role of NO on elastin expression and synthesis by chick aortic SMCs[74]. Although elastin deposition into matrix was not evaluated by them, results showed NO to stimulate tropoelastin mRNA expression, synthesis and release into pooled media by chick cells in a dose-dependent manner (1-100 nM), with the maximum stimulation noted at 100 nM GSNO. In our current study, the excellent elastin matrix yield of ~40% noticed within 1 nM GSNO and EC cocultures was not only relevant to vascular biology studies, but also highly encouraging from tissue engineering and regenerative medicine based stand-points. However, further studies are needed to quantify the changes in elastin gene expressions under these culture conditions.

3.4. Glycosaminoglycan synthesis by HA-SMCs

Studies have shown that chondroitin sulfate and heparan sulfate were the main constituents of sGAGs produced by human aortic SMCs[112]. Suarez et al. have shown that growth factors such as EGF, FGF and VEGF stimulate SMCs to synthesize heparin sulfate in a dose-dependent manner[113]. However, the role of NO or EC cocultures in mediating GAG (sulfated or non-sulfated) synthesis remains unexplored, and this study reports for the first time the dose-dependent effects of NO donors on GAG synthesis by human aortic SMCs. In general, the GAG content within the cell layers and pooled media was quantified as sulfated GAGs (sGAGs) and non-sulfated GAGs (HA). In the absence of EC cocultures, adult HA-SMCs released 16.7 ± 3.2 ng of sGAGs into pooled media on a per cell basis, within GSNO-free cultures (**Fig. 3.3 C**). GSNO addition (1-100 nM) significantly suppressed sGAG release into pooled media when compared to controls ($p < 0.001$). On the other hand, no further benefit of EC coculture to sGAG release into pooled media was noticed within GSNO-free cultures. Within EC cocultures, addition of 1 nM GSNO suppressed sGAG release by SMCs ($p < 0.01$ for 1 nM vs. 0 nM), while 10 and 100 nM GSNO stimulated 1.4–fold and 1.95–fold increases in sGAG release respectively, compared to controls ($p < 0.01$ for 0 nM vs. 10 nM or 100 nM; $p < 0.01$ for 1 nM vs. 10 nM or 100 nM; $p < 0.01$ for 10 nM vs. 100 nM GSNO). Taken together, except within GSNO-free cultures where significant differences were not noticed, coculturing with HA-ECs appeared to stimulate sGAG release by HA-SMCs in a GSNO dose-dependent manner.

The sGAG content deposited within cell matrices seem to reflect the trends observed in matrix elastin synthesis by HA-SMCs. sGAGs presence could not be detected within

HA-SMC cell layers in the absence of EC coculture and GSNO (**Fig. 3.3 D**). However, in the absence of EC cocultures, increasing GSNO concentration from 1-100 nM promoted significant sGAGs deposition in the cell layers in a dose-dependent manner ($p < 0.01$ for 1 nM vs. 10 nM or 100 nM; $p < 0.01$ for 10 nM vs. 100 nM). In the presence of EC cocultures, SMCs deposited 0.62 ± 0.19 ng of sGAGs in the cell layers, on a per cell basis, within GSNO-free cultures. While 1 and 10 nM GSNO did not further promote sGAG deposition into matrix layers within EC cocultures, addition of 100 nM promoted a drastic 7.4-fold increase in sGAG deposition within cell layers, relative to GSNO-free controls ($p < 0.001$ for 100 nM vs. lower GSNO doses). In general, the matrix sGAG yield (ratio of matrix sGAG content to the total sGAGs produced) within SMC cultures ranged between 0 - 10 %, while EC cocultures significantly promoted the same to between 4.2 - 14.5 %. Taken together, results show that 100 nM GSNO stimulated synthesis, release and deposition of sGAGs by HA-SMCs within a biomimetic vascular coculture environment.

The release of non-sulfated GAGs within SMC cultures was different from sGAG trends. SMCs released ~ 2 ± 0.23 pg of HA into pooled media on a per cell basis, in the absence of GSNO and EC cocultures (**Fig. 3.3 E**). Although no further benefits to HA release were realized at lower GSNO dosages (1 and 10 nM), a 1.55-fold increase in HA content was noted at 100 nM GSNO relative to controls ($p < 0.01$ for 100 nM vs. lower doses of GSNO). However, in the presence of EC cocultures, GSNO at 0 nM and 1 nM suppressed HA release by SMCs into pooled media, although this suppression was rescued at higher GSNO dosages. HA release into pooled media was enhanced by 2.4-fold and 3.2-fold, within cultures supplemented with 10 and 100 nM GSNO respectively,

within EC cocultures ($p < 0.001$ for both cases vs. 0 nM cultures). The trends in HA deposition within cell matrix (**Fig. 3.3 F**) mirrors that noted in sGAG deposition within respective cultures. When SMCs were cultured alone, 0.2 ± 0.03 pg of HA was deposited within cell layers on a per cell basis, and addition of GSNO at 1 and 10 nM dosages did not further enhance these deposition levels. However, in the presence of 100 nM GSNO, a 2.44-fold increase in HA deposition was seen ($p < 0.001$ for 100 nM vs. lower GSNO dosages), even in the absence of EC cocultures. Interestingly, no additional benefits of EC coculture to HA matrix deposition was noted at 0 nM or 1 nM GSNO dosages (**Fig. 3.3 F**). A dramatic 2.56-fold and 21.9-fold increase in HA deposition within cell layers was noted when GSNO was supplemented at 10 nM and 100 nM respectively, to SMCs within EC cocultures.

Quantification of HA matrix yield (ratio of HA within cell matrix to total HA synthesis) revealed that the yield increased from ~ 9% within 0-10 nM GSNO cultures to 13.4% within 100 nM GSNO-additive cultures, in the absence of EC cocultures. However, when SMCs were cocultured with ECs, the yields increased from ~ 14% within 0-10 nM GSNO cases to a dramatic 51% within 100 nM GSNO additive cultures. Taken together, results show that 100 nM GSNO might help in the synthesis, release and deposition of hyaluronic acid by human aortic SMCs within biomimetic vascular coculture environment. Our future studies are designed to elucidate the molecular weight ranges of hyaluronic acid fragments synthesized and released under respective conditions.

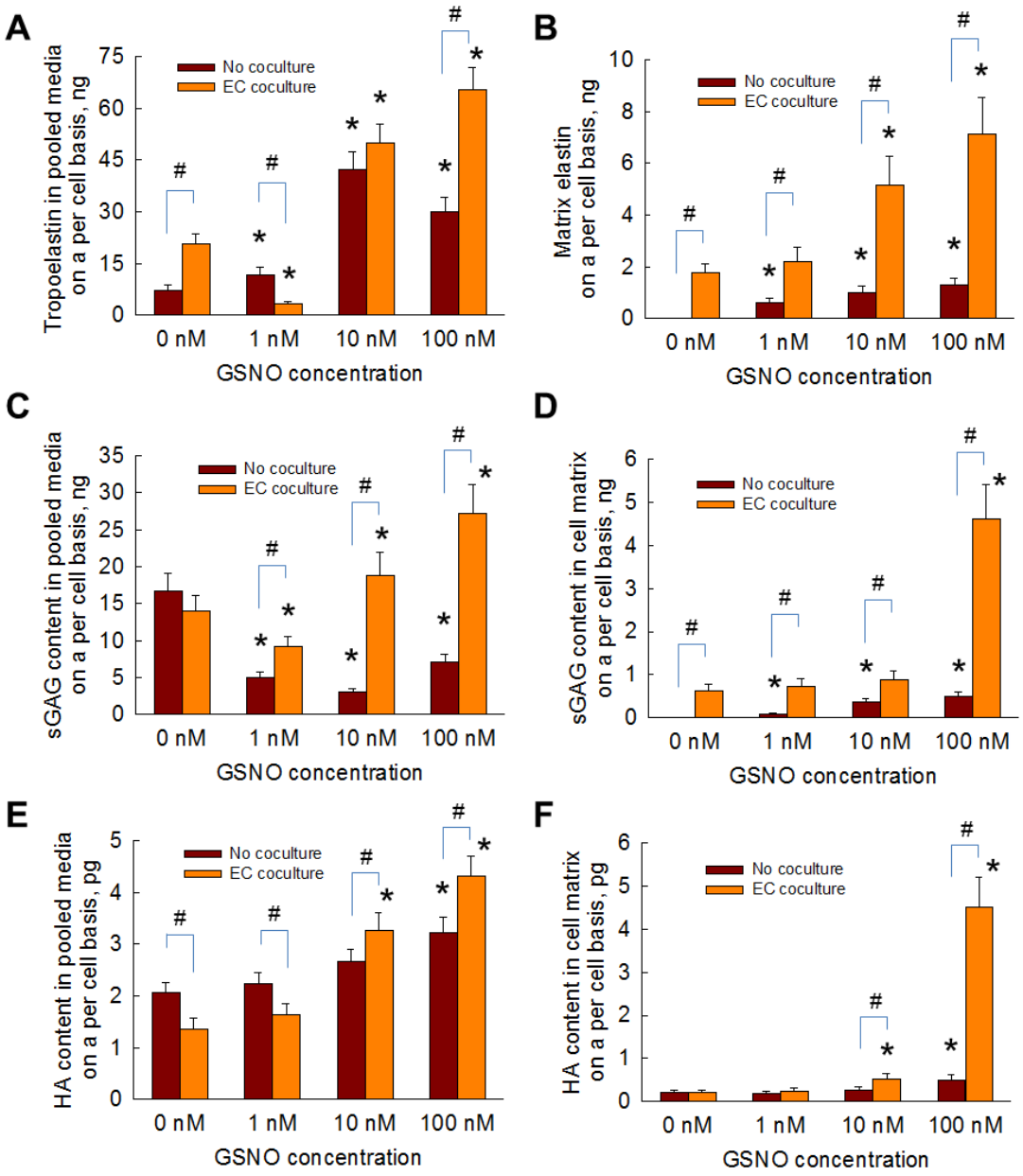

Figure 3.3 When GSNO (0-100 nM) was supplemented to HA-SMC cultures, in the presence or absence of EC cocultures, elastin protein released into pooled media (A) or deposited within cell matrix (B), sulfated GAGs released into pooled media (C) or deposited within cell matrix (D), and HA released into pooled media (E) or deposited within cell matrix (F) was quantified. Data shown represent mean ± standard error of protein synthesis after 21 days of culture, normalized to cell count within respective cases (n = 6/ condition). * indicates $p < 0.05$ compared to GSNO-free cultures; # indicates $p < 0.01$ for no cocultures vs. EC coculture, at a given GSNO dosage.

3.5. LOX enzyme activity

LOX has been shown to play an important role in the crosslinking and maintenance of ECM proteins such as elastin and collagen, and thus expected to participate in ECM remodeling associated with cardiovascular diseases. However, LOX synthesis and activity within adult HA-SMC cultures has not been identified earlier. In this study, the LOX enzymatic activity was quantified within the cell matrix and pooled media to (a) establish the stand-alone and synergistic benefits of GSNO and EC cocultures to LOX activity, and (b) determine whether a correlation exists between LOX enzymatic activity and matrix protein yields within respective cultures. In the absence of EC cocultures and GSNO, LOX activity within pooled media from HA-SMC cultures was quite low (0.076 ± 0.002 nM on a per cell basis; **Fig. 3.4 A**). These basal levels were drastically increased by 10.6-, 12.3- and 20.9–fold, with the addition of 1, 10 and 100 nM GSNO, respectively ($p < 0.001$ for 0 nM vs. higher GSNO dosages; $p < 0.001$ for 1 nM vs. 100 nM; $p < 0.001$ for 10 nM vs. 100 nM). In GSNO-free cultures, coculturing with ECs resulted in a 4.2-fold increase in LOX activity within pooled media, compared to that within SMC cultures ($p < 0.001$). These levels were furthered by 3.9-, 6.2- and 34.8-fold, respectively, with the addition of 1, 10 and 100 nM GSNO to SMC-EC cocultures ($p < 0.001$ vs. controls in all the cases).

The basal levels (at 0 nM GSNO) of LOX activity within cell matrix of SMC cultures (0.067 ± 0.014 nM) increased by 1.65-fold, 2.97-fold and 5.5-fold, respectively, with the addition of 1, 10 and 100 nM GSNO (**Fig. 3.4 B**; $p < 0.01$ for 0 nM vs. higher GSNO doses; $p < 0.01$ for 1 nM vs. higher GSNO doses; $p < 0.01$ for 10 nM vs. 100 nM). EC coculture provided no significant benefit to LOX activity within cell matrix, in the

absence of GSNO. Surprisingly, 1 and 10 nM GSNO inhibited LOX activity within cell matrices in the presence of EC cocultures, while 100 nM GSNO promoted a dramatic 10.6-fold increase ($p < 0.001$ for 100 nM vs. lower dosages). This dramatic increase in LOX activity within cell matrix at 100 nM GSNO dosage, in the presence or absence of EC cocultures, partially explains the multi-fold increases in HA, elastin and sGAG deposition within HA-SMC cell matrices. The only other known report on the effects of NO on LOX synthesis showed a 4.5-fold increase in LOX mRNA expression within chick aortic SMC cultures, with the addition of 100 nM GSNO[74]. We hypothesize that the dramatic increases in LOX activity seen at 100 nM GSNO and EC cocultures in our study might be due to significant increase in LOX mRNA expression, which would be investigated in our future studies.

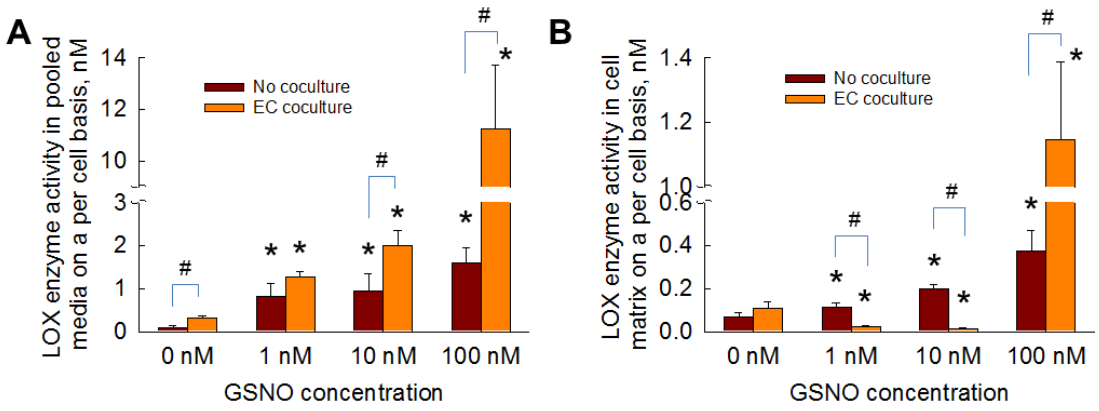

Figure 3.4 LOX enzyme activity within pooled media (A) or within cell matrix (B), when GSNO (0-100 nM) was supplemented to HA-SMC cultures, in the presence or absence of HA-EC cocultures. Data shown represent mean ± standard error of LOX synthesis after 21 days of culture, normalized to cell count within respective cases ($n = 6$ per condition). * indicates $p < 0.05$ compared to GSNO-free cultures; # indicates $p < 0.01$ for no cocultures vs. EC coculture, at a given GSNO dosage.

3.6. Release of MMPs-2, 9 and TIMP

In this study, the amounts of MMPs-2, 9 and TIMP into pooled media was quantified on a per cell basis (**Fig. 3.5**). The amounts of these enzymes were insignificant to be accurately quantifiable in cell matrix. In the absence of EC coculture and GSNO, HA-SMCs released ~ 25 pg of MMP-2 on a per cell basis (**Fig. 3.5 A**). The addition of 1-100 nM GSNO to SMC cultures suppressed MMP-2 release by 50-70% on a per cell basis ($p < 0.01$ for 0 nM vs. higher GSNO dosages; $p < 0.01$ for 1 nM vs. higher GSNO dosages). Coculturing with ECs suppressed MMP-2 release by SMCs, in the absence of GSNO. The average MMP-2 release within EC cocultures increased from 11.6 pg within controls (0 nM GSNO) to ~ 15 pg within 1 nM GSNO and to ~ 26 pg within 10 and 100 nM GSNO cultures ($p < 0.01$ for 0 nM vs. 10 or 100 nM GSNO, within cocultures). On the other hand, MMP-9 levels increased marginally within SMC cultures in the presence of GSNO, compared to GSNO-free cultures (**Fig. 3.5 B**; $p < 0.01$ for 0 nM vs. higher GSNO dosage; $p < 0.01$ for 1 nM vs. 100 nM; $p < 0.01$ for 10 nM vs. 100 nM). Within EC cocultures, MMP-9 levels were inhibited at lower GSNO concentrations (0-10 nM) compared to SMC cultures, although 100 nM GSNO increased MMP-9 release by SMCs for reasons not clear at this stage.

In the absence of cocultures and GSNO, HA-SMCs produced 1.57 ± 0.39 pg of TIMP-1 on a per cell basis (**Fig. 3.5 C**). These TIMP-1 levels were significantly suppressed by addition of 1 nM GSNO ($p < 0.01$ for 1 nM vs. 0 nM GSNO), while 10 and 100 nM GSNO offered only marginal benefits compared to controls. Within EC cocultures, although 1 nM GSNO did not enhance basal levels of TIMP-1 release by HA-SMCs (3.05 ± 0.6 pg per cell; $p = 0.22$ for 1 nM vs. 0 nM), 10 and 100 nM GSNO

promoted 1.96-fold and 2.1-fold increases in TIMP-1 release into pooled media ($p < 0.001$ vs. 0 nM GSNO in both cases; $p < 0.001$ vs. 1 nM GSNO in both the cases). In general, higher levels of TIMP-1 release were noted in cocultures compared to when SMCs cultured alone. Taken together, these results suggest that (a) exogenous GSNO supplementation suppressed MMP-2 and marginally enhanced MMP-9 release when HA-SMCs were cultured alone, (b) MMPs levels increased within cocultures with increasing GSNO, and (c) higher GSNO dosages enhanced the release of TIMP-1 by HA-SMCs in the presence of HA-EC cocultures.

Matrix metalloproteinases, specifically MMP-2 and MMP-9, play an important role in degrading basement membrane and ECM microenvironment, thus facilitating SMC migration during injury or disease (atherosclerosis, aneurysms, angioplasty, etc.) conditions in vasculature. On the other hand, naturally-available tissue inhibitors of MMPs (e.g., TIMP-1) released by SMCs contribute to reduction in such ECM breakdown, SMC migration and inflammation levels. Thus, a balance (or lack thereof) of these two components contributes to changes in SMC phenotype from quiescent to migratory and invasive nature. However, the specific levels of MMPs and TIMPs synthesized by adult human vascular SMCs within 3D biomimetic cultures are not known. Besides, very few studies explored the role of nitric oxide in regulating MMPs and TIMP levels within vasculature, under healthy or diseased conditions. In a recent study, Dey et al. reported on the molecular pathways involved in NO-mediated release of MMPs and TIMP by rat aortic SMCs *in vitro*[114]. They noted that in the presence of DETA NONOate, an NO donor, rat SMCs synthesized and secreted more MMP-2 and less amounts of MMP-9, while TIMP-2 levels increased as well. We hypothesize that the

higher levels of MMPs and TIMP-1 noted within cocultures might be due to the combined release from SMCs and ECs, although further experiments are needed to quantify their release from ECs alone, and the effects of paracrine signaling between HA-ECs and HA-SMCs.

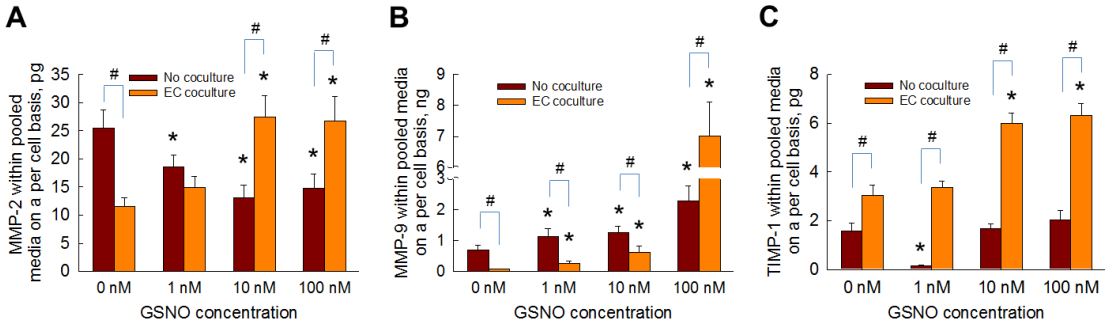

Figure 3.5 When GSNO (0-100 nM) was supplemented to HA-SMC cultures, in the presence or absence of EC cocultures, the release of MMP-2 (A), MMP-9 (B), and TIMP-1 (C) into pooled media was quantified. Data shown represent mean ± standard error of protein synthesis after 21 days of culture, normalized to cell count within respective cases (n = 3 per condition). * indicates $p < 0.05$ compared to GSNO-free cultures; # indicates $p < 0.01$ for no cocultures vs. EC coculture, at a given GSNO dosage.

3.7. Immunofluorescence labeling of Elastin, Fibrillin and LOX

Immunofluorescence images under these culture conditions qualitatively support the elastin and LOX deposition within cell matrix layers discussed above. When SMCs were cultured alone within 3D scaffolds (**Fig. 3.6**), significantly higher staining for matrix elastin was noted within cultures supplemented with 10 and 100 nM GSNO, compared to that at 0 and 1 nM GSNO. Similar increases in LOX deposition was noted within cultures receiving higher dosages of GSNO. Although coculturing with HA-ECs resulted in higher amounts of matrix elastin deposition at all GSNO dosages, the staining intensity was more pronounced at higher GSNO concentrations (10 and 100 nM; **Fig. 3.7**). In

strong agreement with quantitative data, a robust staining for LOX within 100 nM GSNO additive cultures was apparent, when SMCs were cocultured with ECs. Images from negative control cultures (stained without primary antibody) showed no coloration (data not shown). In general, staining for these proteins was evident in different planes of focus within these 3D gels. These data are in broad agreement with the quantitative data on matrix elastin (**Fig. 3.3 B**) and LOX activity (**Fig. 3.4 B**) within respective cultures. While staining for fibrillin expression could be seen within all the cases, it was modest and seems to be confined to the periphery of the cells. It also raises the possibility that adult human aortic SMCs do not produce much fibrillin, although further studies are needed to precisely measure the ability of HA-SMCs to synthesize and deposit protein fibers (fibrillin, fibulins, MAGPs, etc.) important for elastin assembly and maturation. Our current studies are geared towards elucidating the ultrastructure of the matrix proteins (e.g., fibrillar, co-localization), using characterization tools such as transmission electron microscopy.

It could be seen that the combined amount of elastin and GAGs (quantified in **Figs. 3.3** and **3.4**), in both pooled media and cell matrix, and is much lower than that quantified from BCA assay (**Fig. 3.2**). This suggests that in addition to elastin and GAGs, numerous other proteins such as collagens and proteoglycans, might be released and deposited by HA-SMCs within 3D scaffolds, which we intend to quantify in our future studies. Intuitively, we speculate that changing the composition or stiffness of the 3D scaffold (2 mg/ml type-1 collagen) used in this study, might influence the cell proliferation and matrix synthesis outcomes by HA-SMCs in the presence of GSNO. Besides, results from this study pose a few challenging questions: Does exogenous GSNO addition stimulate

endogenous NO release by HA-ECs, and if so, is there a dose-dependency affect? At 100 nM GSNO addition, what cytokines and chemokines are being released by SMCs and/or ECs, and are they influencing the multi-fold increases noted in protein release and matrix deposition? Our current studies are geared towards investigating these phenomena within our culture system. Nevertheless, a systematic understanding of the complex pathways involved in NO-mediated SMC signaling is essential in formulating pharmaceutical approaches for the treatment of vascular degenerative diseases.

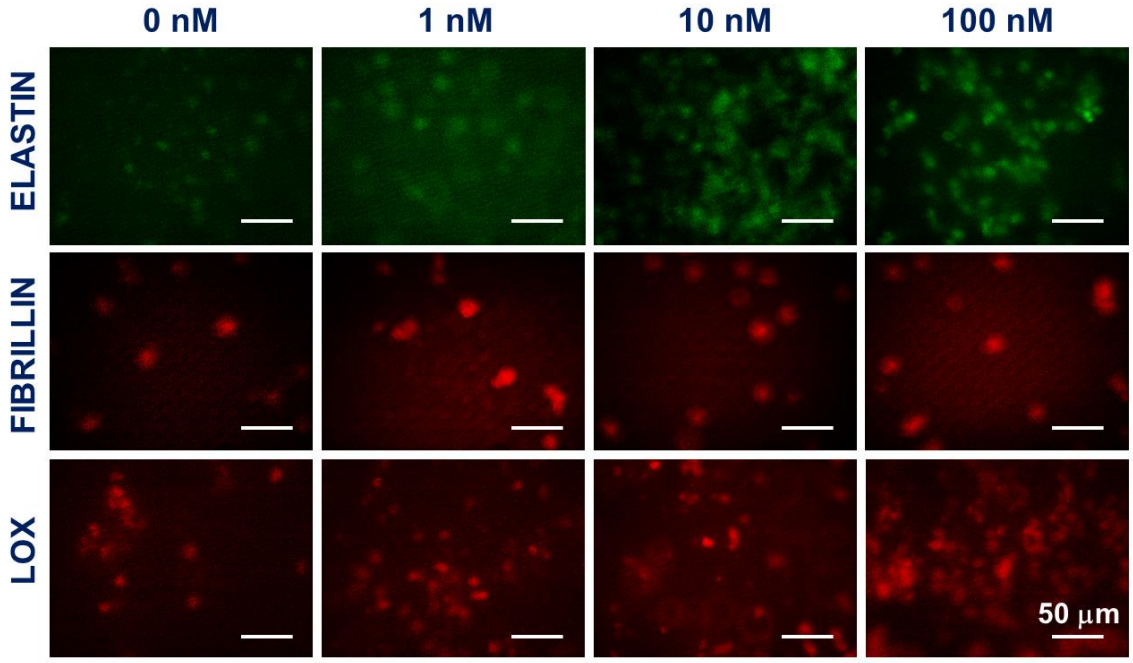

Figure 3.6 Immunofluorescence images of elastin, fibrillin and LOX proteins deposited by HA-SMCs within cell matrix layers, in the presence of GSNO (0-100 nM). HA-SMCs were cultured alone within 3D scaffolds, in the absence of cocultures with endothelial cells.

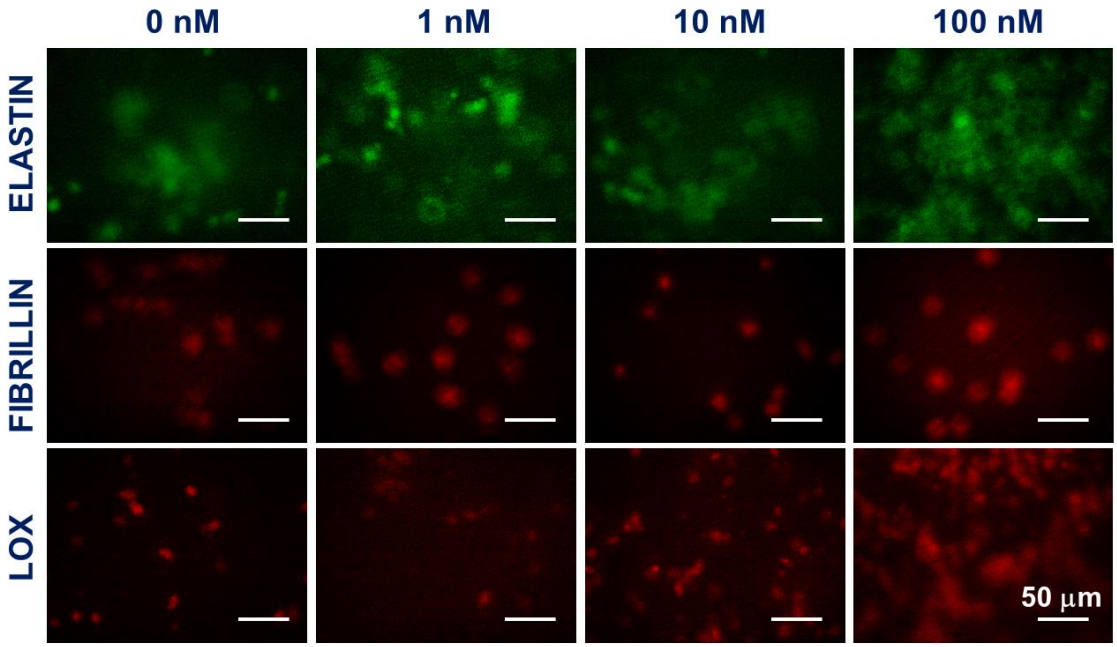

Figure 3.7 Immunofluorescence images of elastin, fibrillin and LOX proteins deposited by HA-SMCs within cell matrix layers, in the presence of GSNO (0-100 nM). HA-SMCs were cultured within 3D scaffolds, in the presence of cocultures with human aortic endothelial cells.

CHAPTER IV

RESULTS AND DISCUSSION: ANEURYSMAL HUMAN SMCS IN 2D AND 3D CULTURES

4.1. Aneurysmal HA-SMC proliferation

For 2D and 3D cultures, we seeded at roughly 10,000 cells in each well, as measured by hemocytometer analysis. However, we performed a quantitative cell density analysis on day 1 after seeding to accurately measure the number of cells seeded and for both cases ~7,800 cells were seeded in each case. The proliferation of diseased HA-SMCs cultured in 2D and 3D, both in the presence and absence of GSNO is shown in **Fig. 4.1**. In the absence of GSNO the SMCs proliferated 2.8-fold in 2D, and roughly doubled in 3D gels ($p < 0.05$ vs. 2D control) at 21 days cultured. The addition of 100 nM GSNO decreased the SMC proliferation in both 2D and 3D to 2.05-fold ($p < 0.05$ vs. 2D control) and 1.3-fold ($p < 0.05$ vs. 2D control, $p < 0.05$ vs. 3D control) respectively.

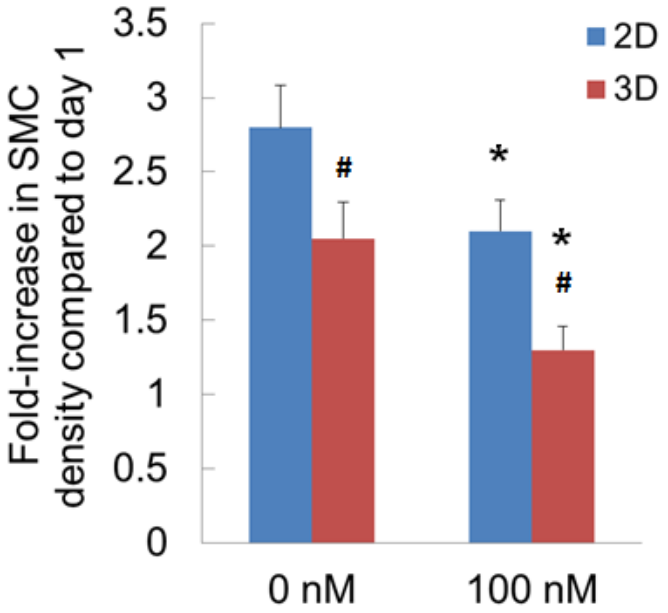

Figure 4.1 (A) Fold increase in human aneurysmal SMC density within 3D cultures supplemented with GSNO (0-100 nM). Data shown represent mean ± standard error of cell count after 21 days of culture, normalized to initial seeding density (n = 3/ condition). * indicates $p < 0.01$ compared to GSNO-free cultures; # indicates $p < 0.01$ for 2D vs. 3D, at a given GSNO dosage.

It is also important to note that the GSNO dose used in this study was identified from our previous study (Chapter III) where a range of GSNO doses were tested to upregulate the ECM components. Just like our past study, we did not investigate the NO activity and release rates from GSNO within culture media at neutral pH, as this data has been previously reported[94,95]. Previous studies utilizing the aneurysmal SMCs show ~4.2 fold increase in cell proliferation under normal conditions in 2D[115]. Alternately, in a study involving rat aneurysm SMCs proliferated 2.5± 0.32 fold over 21 days[116]. The data obtained in this study was found to be between the results obtained in previous experiments in 2D and the absence of GSNO. There is still no work that looks at the addition of GSNO in 3D cultures of aneurysmal SMCs and the data obtained in this

experiment shows a slight decrease in the proliferation of SMCs when compared to the data shown in Chapter III.

4.2. Total protein synthesis by aneurysmal HA-SMCs

The total protein amount synthesized by the diseased HA-SMCs, cultured in both 2D and 3D, under the presence or absence of GSNO is quantified in **Fig. 4.2**. The total protein amounts were quantified as two separate components: released into the pooled spent media and the protein deposited in the cell matrix. Diseased HA-SMCs synthesized and deposited 16.2 ± 2.4 ng and 266.4 ± 40 ng ($p < 0.05$ vs. 2D control) of protein, on a per cell basis, in 2D and 3D cultures respectively. With the addition of GSNO there was a significant multi-fold increase in the total protein in the cell matrix in both the 2D and 3D cultures, compared to cultures that lacked GSNO ($p < 0.05$ vs. 2D control and $p < 0.05$ vs. 3D control). Also, there was a significant difference between the total protein on a per cell basis that was deposited in the cell matrix between the 2D and 3D cultures in the presence of GSNO ($p < 0.05$ vs. GSNO-free controls in both 2D and 3D). The total protein synthesized on a per cell basis and released into the pooled spent media in the absence of GSNO was 16.8 ± 2.5 µg and 37.9 ± 5.7 µg ($p < 0.05$ for 3D vs. 2D) 2D and 3D cultures, respectively. Similar to that seen in the cell matrix, there was a significant increase in the total protein synthesized and released into the pooled spent media with the addition of GSNO: 34.6 ± 5.2 µg in 2D cultures and 52.7 ± 7.9 µg within 3D cultures, respectively ($p < 0.05$ vs. 2D control, $p < 0.05$ vs. 3D control and $p < 0.05$ vs. 2D with GSNO).

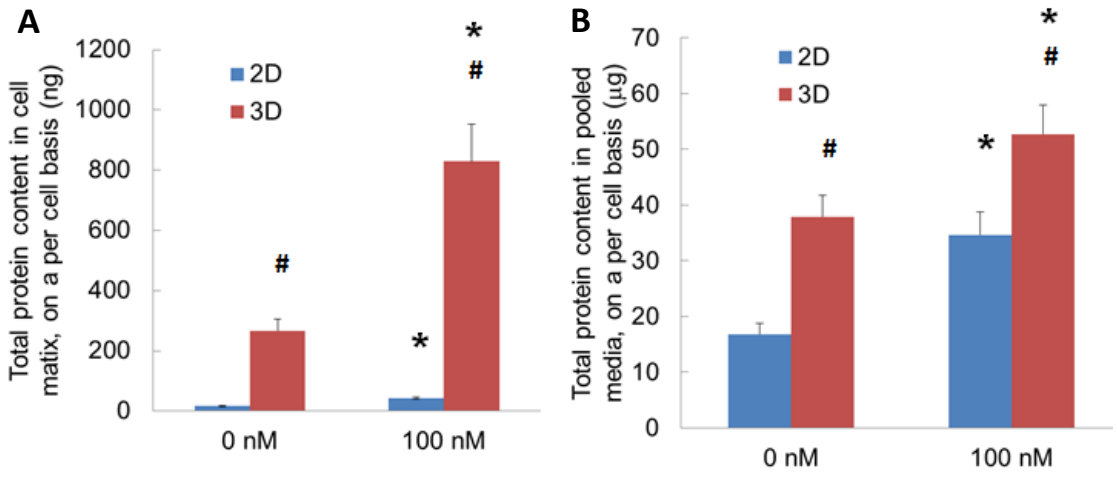

Figure 4.2 Total protein amounts deposited within cell matrix (A) or released into pooled media (B), when GSNO (0, 100 nM) was supplemented to human aneurysmal SMC cultures, in 2D and 3D cultures. Data shown represent mean ± standard error of protein synthesis after 21 days of culture, normalized to cell count within respective cases (n = 6/ condition). * indicates $p < 0.01$ compared to GSNO-free cultures; # indicates $p < 0.01$ for 2D vs. 3D, at a given GSNO dosage.

4.3. Elastin synthesis and deposition by aneurysmal HA-SMCs

The total elastin synthesized by diseased HA-SMCs was quantified as that released into the pooled spent media (i.e., tropoelastin) or that deposited into the cell layers (i.e., matrix elastin). The elastin deposited into the cell matrix was 0.56 ± 0.08 pg in 2D cultures, and 0.81 ± 0.12 pg within 3D cultures ($p < 0.05$ for 2D vs. 3D). Upon addition of GSNO, two opposite trends were noticed. The 2D cultures induced less matrix elastin in the cell layers than in the absence of GSNO ($p < 0.05$ vs. 2D control), while the 3D cultures promoted deposition of significantly higher matrix elastin amounts in the presence of GSNO ($p < 0.05$ vs. 3D control; $p < 0.05$ for 3D vs. 2D with GSNO). The elastin deposited in the cell layers (i.e., matrix yield) is significantly lower compared to the elastin released into the pooled media. Within GSNO-free controls, elastin released into the pooled media (tropoelastin) was 152.8 ± 22.9 pg in 2D and 169.23 ± 25.4 pg in

3D, which are not significantly different. When GSNO was added, the 2D cultures did not have a significant change in the tropoelastin released, while there was a larger increase in the release of tropoelastin within 3D cultures ($p < 0.05$ vs. 3D control; $p < 0.05$ for 3D vs. 2D with GSNO).

From the data shown in **Figs. 4.3 A** and **B**, the matrix elastin yield (ratio of matrix elastin to the total elastin produced) within aneurysm HA-SMC cultures was calculated. When aneurysm SMCs were cultured in 2D, the matrix elastin yields were 0.4% and 0.08% within 0 nM and 100 nM GSNO additive-cultures, respectively. However, 3D cultures modest enhanced matrix elastin yields, both in the presence or absence of GSNO. The matrix elastin yield within 0 nM and 100 nM GSNO additive cultures were 0.5% and 0.8%, respectively.

In this study we cultured human aneurysmal SMCs in both 3D collagen scaffolds and on collagen-coated 2D plastic plates. The 3D cultures allow us to mimic physiological conditions and enable future tissue engineering based approaches for in situ elastin regeneration. We noted an increase in tropoelastin production as well as matrix elastin deposition within 3D cultures under the presence of GSNO cocultures. These results confirm our hypothesis that delivering exogenous NO cues to aneurysmal SMCs might help promote protein synthesis, release and deposition within 3D cultures, in addition to regulating their proliferation behavior. Rat aneurysmal SMCs under the presence of different exogenously supplemented cues showed a 1 to 1.6 fold increase in the total amount of elastin compared to 2D culture controls[116]. Similar results were observed in our 2D and 3D cultures with the 3D culture being similar to the largest increase observed in previous studies.

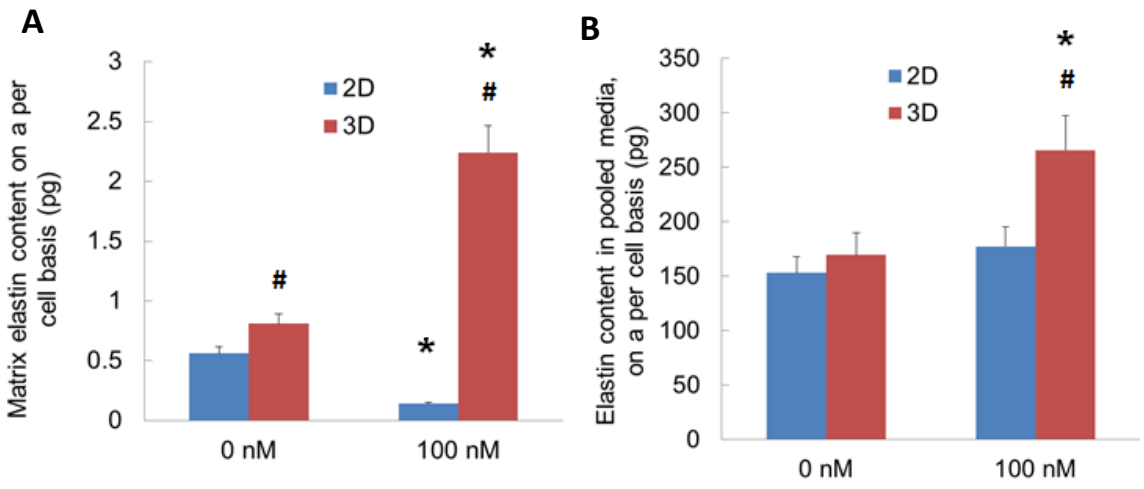

Figure 4.3 When GSNO (0, 100 nM) was supplemented to human aneurysmal SMC cultures, in 2D or 3D cultures, elastin protein released into pooled media (A) or deposited within cell matrix (B). Data shown represent mean ± standard error of protein synthesis after 21 days of culture, normalized to cell count within respective cases (n = 6/ condition). * indicates $p < 0.01$ compared to GSNO-free cultures; # indicates $p < 0.01$ for 2D vs. 3D, at a given GSNO dosage.

4.4. Glycosaminoglycan synthesis by aneurysmal HA-SMCs

Our past study (Chapter III) reported for the first time the dose-dependent effects of NO donors on the GAG synthesis by human aortic SMCs[117]. The total sGAG synthesized by the diseased HA-SMCs, cultured in both 2D and 3D, under the presence or absence of GSNO is quantified in **Fig. 4.4**. The sGAGs deposited into the cell matrix in the absence of GSNO is 0.14 ± 0.02 pg within 2D cultures, and 0.86 ± 0.13 pg within 3D cultures ($p < 0.05$ vs. 2D control). The addition of GSNO increased the deposition of sGAGs on a per cell basis in both the 2D and 3D cultures: 0.38 ± 0.06 pg ($p < 0.05$ vs. 2D control) and 1.3 ± 0.2 pg ($p < 0.05$ vs. 3D control; $p < 0.05$ vs. 2D with GSNO), respectively. Similar trends were seen in the sGAGs released into the pooled media, although the amounts were two orders of magnitude higher. The sGAGs released into the

pooled media in the absence of GSNO is 15.8 ± 2.4 pg in 2D cultures, and 36.4 ± 5.5 pg within 3D cultures ($p < 0.05$ vs. 2D control). The addition of GSNO increased the release of sGAGs on a per cell basis in both the 2D and 3D cultures: 34.4 ± 5.2 pg ($p < 0.05$ vs. 2D control) and 62.9 ± 9.4 pg ($p < 0.05$ vs. 3D control and $p < 0.05$ vs. 2D with GSNO) respectively.

From the data shown in **Figs. 4.4 A** and **B**, the matrix GAG yield (ratio of matrix GAG to the total GAG produced) within aneurysm HA-SMC cultures was calculated. When aneurysm SMCs were cultured in 2D, the matrix GAG yields were 0.9% and 2.3% within 0 nM and 100 nM GSNO additive-cultures, respectively. 3D cultures did not show any significant enhancement of matrix GAG yields, both in the presence or absence of GSNO. The matrix GAG yield within 0 nM and 100 nM GSNO additive cultures were 1.1% and 2%, respectively.

The release of non-sulfated GAGs (i.e., HA) synthesized by the diseased HA-SMCs, cultured in both 2D and 3D, under the presence or absence of GSNO is quantified in **Fig. 4.5**. HA deposited into the cell matrix in the absence of GSNO is 0.36 ± 0.05 pg in 2D cultures and 0.57 ± 0.08 pg in 3D cultures ($p < 0.05$ vs. 2D control). The addition of GSNO modestly increased the deposition of HAs on a per cell basis in both the 2D and 3D cultures: 0.51 ± 0.08 pg ($p < 0.05$ vs. 2D control) and 0.77 ± 0.11 pg ($p < 0.05$ vs. 3D control and $p < 0.05$ vs. 2D with GSNO) respectively. Similar trends were seen in the HA released into the pooled media. HA released into the pooled media in the absence of GSNO is 22.86 ± 3.4 pg within 2D cultures, and 27.66 ± 4.1 pg within 3D cultures, which are not significantly different. The addition of GSNO increased the release of HA on a per cell basis in both 2D and 3D cultures: 29.75 ± 4.5 pg ($p < 0.05$ vs. 2D control)

and 40.71 ± 6.1 pg (p < 0.05 vs. 3D control and p < 0.05 vs. 2D with GSNO) respectively.

From the data shown in **Figs. 4.5 A** and **B**, the matrix HA yield (ratio of matrix HA to the total HA produced) within aneurysm HA-SMC cultures was calculated. When aneurysm SMCs were cultured in 2D, the matrix HA yields were 1.6% and 1.7% within 0 nM and 100 nM GSNO additive-cultures, respectively. However, 3D cultures modest enhanced matrix HA yields, both in the presence or absence of GSNO. The matrix HA yield within 0 nM and 100 nM GSNO additive cultures were 2% and 1.9%, respectively.

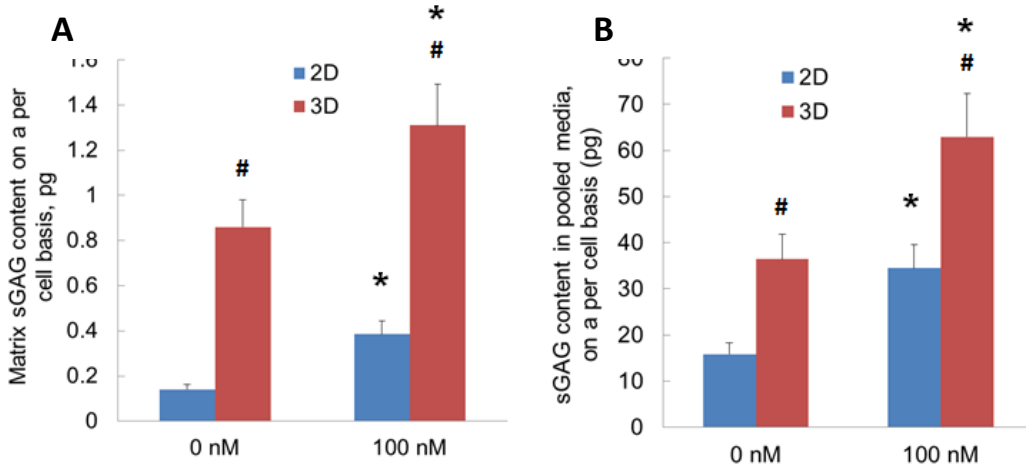

Figure 4.4 When GSNO (0, 100 nM) was supplemented to human aneurysmal SMC cultures, in 2D or 3D cultures, sulfated GAGs released into pooled media (A) or deposited within cell matrix (B). Data shown represent mean ± standard error of protein synthesis after 21 days of culture, normalized to cell count within respective cases (n = 6/ condition). * indicates p < 0.01 compared to GSNO-free cultures; # indicates p < 0.01 for 2D vs. 3D, at a given GSNO dosage.

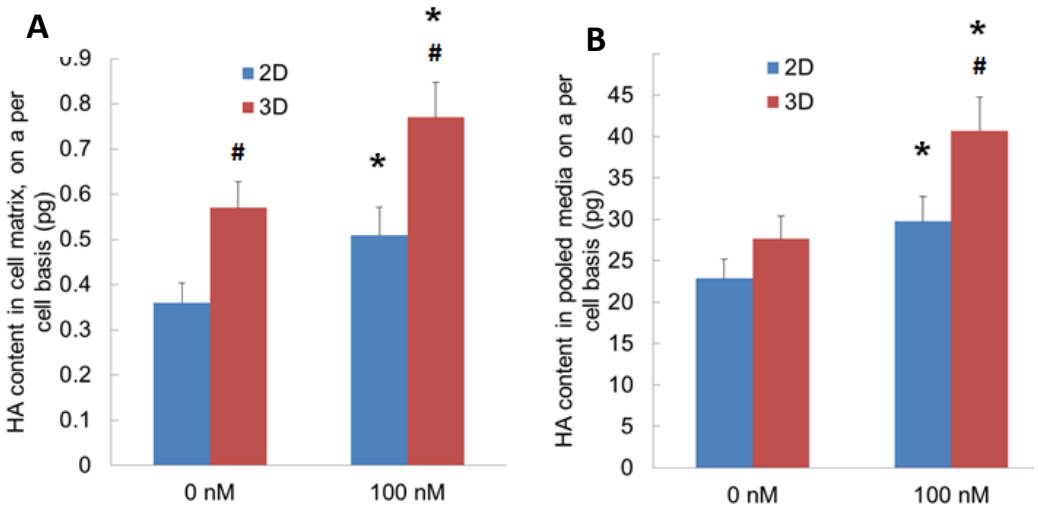

Figure 4.5 When GSNO (0, 100 nM) was supplemented to human aneurysmal SMC cultures, in 2D or 3D cultures, HA released into pooled media (A) or deposited within cell matrix (B). Data shown represent mean ± standard error of protein synthesis after 21 days of culture, normalized to cell count within respective cases (n = 6/ condition). * indicates $p < 0.01$ compared to GSNO-free cultures; # indicates $p < 0.01$ for 2D vs. 3D, at a given GSNO dosage.

4.5. LOX- protein synthesis and activity

The activity of LOX-proteins synthesized by aneurysmal HA-SMCs in both 2D and 3D cultures can be seen in **Fig. 4.6**. The LOX proteins deposited in the cell layers in the absence of GSNO were 0.025 ± 0.004 pM within 2D cultures and 0.11 ± 0.016 pM in 3D cultures ($p < 0.001$ for 3D vs. 2D). While the addition of GSNO to 2D cultures did not induce a significant change in LOX activity within cell matrix, it induced ~2.5-fold increase in LOX activity within 3D cultures ($p < 0.05$ vs. 3D control; $p < 0.0001$ vs. 2D with GSNO). When considering the LOX activity within pooled media under no exogenous GSNO addition, there was a large difference in the amounts quantified in 2D vs. 3D cultures: 0.185 ± 0.03 pM and 2.76 ± 0.4 pM ($p < 0.05$ vs. 2D control) respectively. Surprisingly, the addition of GSNO to 3D cultures did not significantly

alter LOX activity, compared to GSNO absence. However, within 2D cultures, LOX activity increased multifold with the addition of GSNO ($p < 0.001$ vs. 2D control). It is important to note that the LOX released into the pooled media in the 3D cultures was still significantly larger than the 2D cultures ($p < 0.05$ vs. 2D with GSNO). Rat aneurysmal SMCs under the presence of different exogenously supplemented cues showed a 1 to 1.7 fold increase in the total amount of LOX proteins compared to 2D culture controls[116]. Similar results were observed in our 3D cultures. However, with ~12 fold increase the 2D culture in this experiment shows a large upregulation of the LOX protein when under the influence of GSNO compared to other exogenously supplemented cues in the rat model.

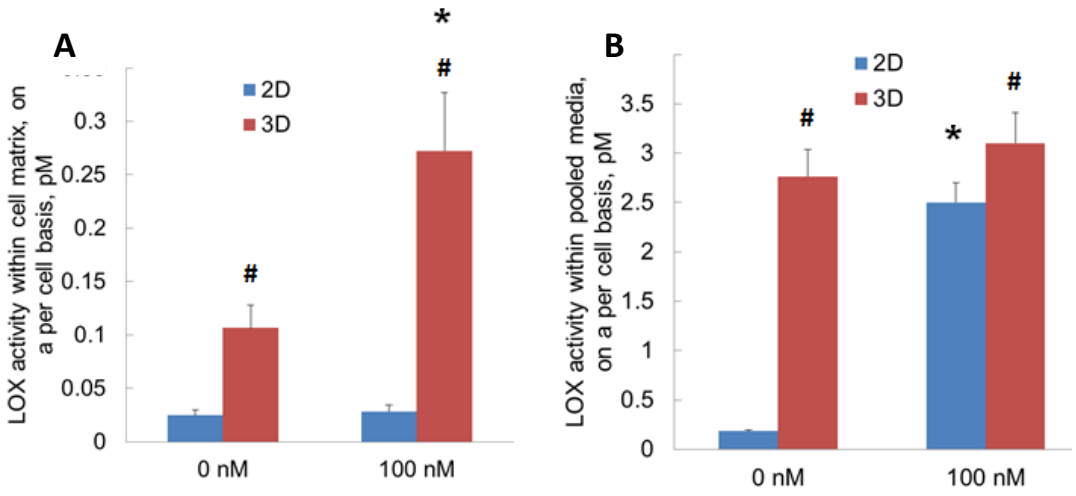

Figure 4.6 LOX enzyme activity within pooled media (A) or within cell matrix (B), when GSNO (0, 100 nM) was supplemented to human aneurysmal SMC cultures, in 2D and 3D cultures. Data shown represent mean ± standard error of LOX synthesis after 21 days of culture, normalized to cell count within respective cases ($n = 6$ per condition). * indicates $p < 0.01$ compared to GSNO-free cultures; # indicates $p < 0.01$ for 2D vs. 3D, at a given GSNO dosage.

4.6. MMPs-2, 9 and TIMP-1 protein synthesis

The production of all MMPs and TIMPs for their release into the pooled spent media in 2D and 3D can be seen in **Fig. 4.7**. The deposition of these proteins in the cell matrix was too low to be reported. As for the MMP-2 release into the pooled media, the control levels quantified were not significantly different from each other in 2D (5.99 ± 0.9 pg) vs. 3D (7.61 ± 1.1 pg) cultures. With the addition of GSNO, although the 2D cultures did not induce any significant change, there was a significant increase in MMP-2 release within 3D cultures ($p < 0.05$ vs. 3D control; $p < 0.05$ vs. 2D with GSNO). Similar trends were noted for MMP-9 release as well. Although no significantly different values were noted within GSNO-free 2D and 3D cultures, the addition of GSNO induced a significantly higher increase in the release of MMP-9 within 3D cultures compared to the 3D control ($p < 0.05$vs. 3D control). TIMP-1 release into the pooled media was quantified at 0.53 ± 0.08 pg in 2D and 0.68 ± 0.1 pg in 3D cultures, in the absence of GSNO. The addition of GSNO induced a significant increase in both the 2D and 3D cultures. Within 2D cultures, it increased to 0.71 ± 0.1 pg ($p < 0.05$ vs. 2D control), while within 3D cultures it increased to 1.82 ± 0.27 pg ($p < 0.05$ vs. 3D control and $p < 0.05$ vs. 2D with GSNO). Rat aneurysmal SMCs under the presence of different exogenously supplemented cues showed a 1.1 to 1.6 and 0.9 to 2 fold increase in the total amount of MMP-2 and MMP-9, respectively, compared to 2D culture controls[116]. Studies have shown that NO upregulated MMP enzymes in melanoma cell lines as well as in pulmonary tissue, and although the exact cause is still unknown it is believed that NO molecule or one of the partially reduced forms was responsible for that result[118,119].

The addition of GSNO showed to follow the same trends as the hyaluronan oligomers and TGF-ß1 for both 2D and 3D cultures.

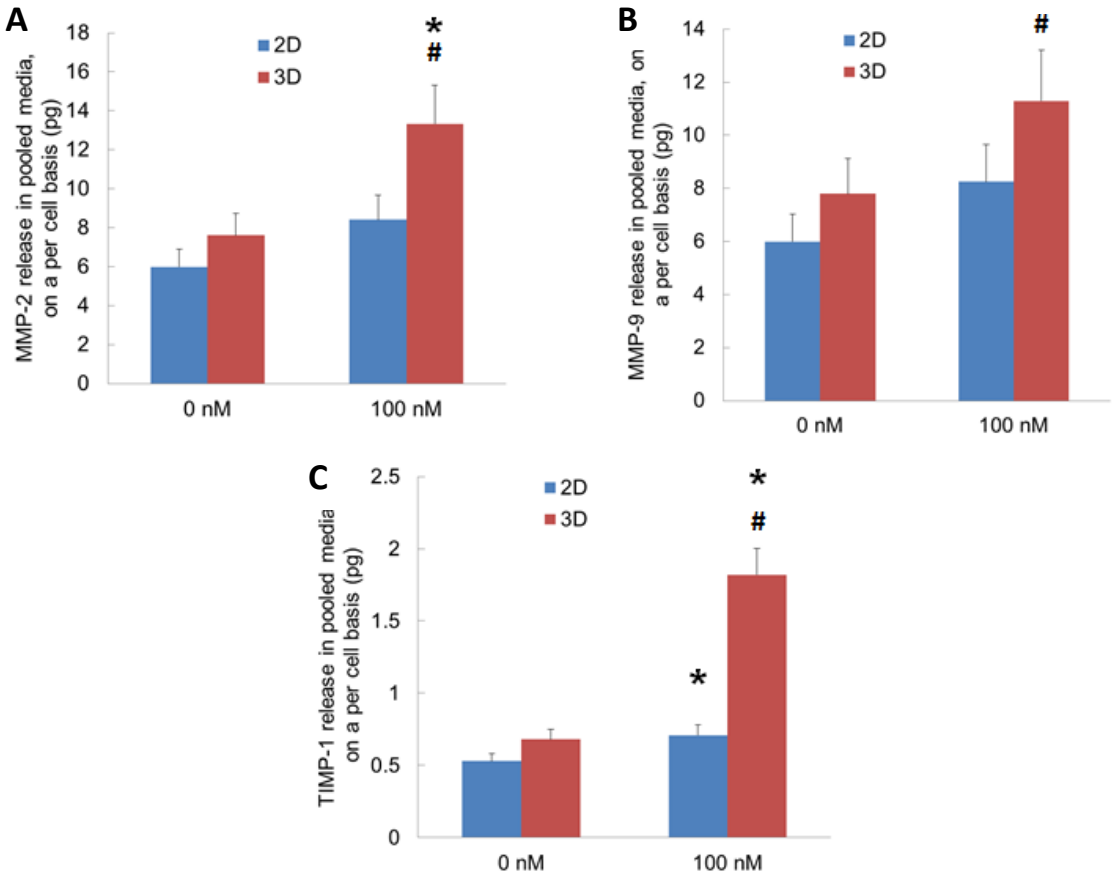

Figure 4.7 When GSNO (0, 100 nM) was supplemented to human aneurysmal SMC cultures, in 2D and 3D cultures, the release of MMP-2 (A), MMP-9 (B), and TIMP-1 (C) into pooled media was quantified. Data shown represent mean ± standard error of protein synthesis after 21 days of culture, normalized to cell count within respective cases (n = 3 per condition). * indicates $p < 0.01$ compared to GSNO-free cultures; # indicates $p < 0.01$ for 2D vs. 3D, at a given GSNO dosage.

4.7. Immunofluorescence labeling of Elastin, Fibrillin and LOX

Immunofluorescence images under these culture conditions qualitatively support the elastin and LOX deposition within cell matrix layers discussed above. When aneurysmal SMCs were cultured alone within 3D scaffolds, significantly higher staining for matrix elastin was noted within cultures supplemented with 100 nM GSNO, compared to that at

0 nM GSNO and both 2D scaffold conditions (**Fig. 4.8**). Similar increases in LOX deposition was noted within 3D cultures receiving the dose of GSNO. In strong agreement with quantitative data, a robust staining for LOX within 100 nM GSNO additive cultures was apparent, for both the 2D and 3D cultures. Images from negative control cultures (stained without primary antibody) showed no coloration (data not shown). In general, staining for these proteins was evident in different planes of focus within these 3D gels. These data are in broad agreement with the quantitative data on matrix elastin (**Fig. 4.3**) and LOX activity (**Fig. 4.6**) within respective cultures. While staining for fibrillin and LOX expression could be seen within all the cases, it was modest and seems to be confined to the periphery of the cells. It also raises the possibility that diseased adult human aortic SMCs do not produce much fibrillin or LOX, although further studies are needed to precisely measure the ability of HA-SMCs to synthesize and deposit protein fibers (fibrillin, fibulins, MAGPs, etc.) important for elastin assembly and maturation.

It could be seen that the combined amount of elastin and GAGs (quantified in **Figs. 4.3** and **4.4**), in both pooled media and cell matrix, and is much lower than that quantified from BCA assay (**Fig. 4.2**). This suggests that in addition to elastin and GAGs, numerous other proteins such as collagens and proteoglycans, might be released and deposited by HA-SMCs within 2D and 3D scaffolds, which we intend to quantify in our future studies.

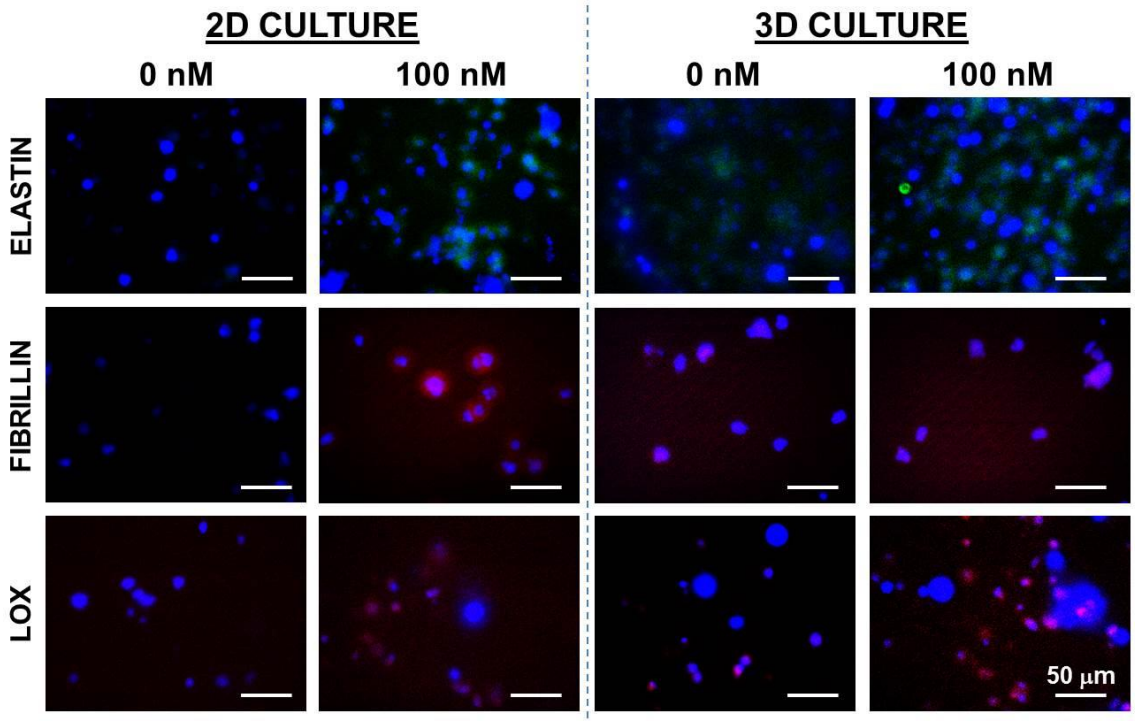

Figure 4.8 Immunofluorescence images of elastin, fibrillin and LOX proteins deposited by HA-SMCs within cell matrix layers, in the presence of GSNO (0, 100 nM). HA-SMCs were cultured alone within 2D and 3D scaffolds.

4.8. Dimension measurements of both aneurysmal and healthy SMC

The dimensions of healthy and diseased SMCs within 2D cultures lacking any GSNO are shown in. This data shows that in diseased conditions, the overall area and perimeter significantly increased when compared to the healthy condition. It is important to note that these cells came from different donors which can lead to a difference in size among the cells.

Table 4.1 Summary of cell dimension measurements.

Healthy	Area (µm2)	Perim. (µm)	Diseased	Area (µm2)	Perim. (µm)
1	5395.892	517.88	**1**	6817.193	864.848
2	3341.64	376.03	**2**	32128	1866.53
3	4019.314	431.657	**3**	4449.49	574.567
4	8869.18	668.517	**4**	6602.274	580.818
5	3349.1	512.516	**5**	3270.119	442.134
6	7125.839	689.759	**6**	3679.142	667.762
Average	5350.160833	532.7265	**Average**	9491.03633	832.7765

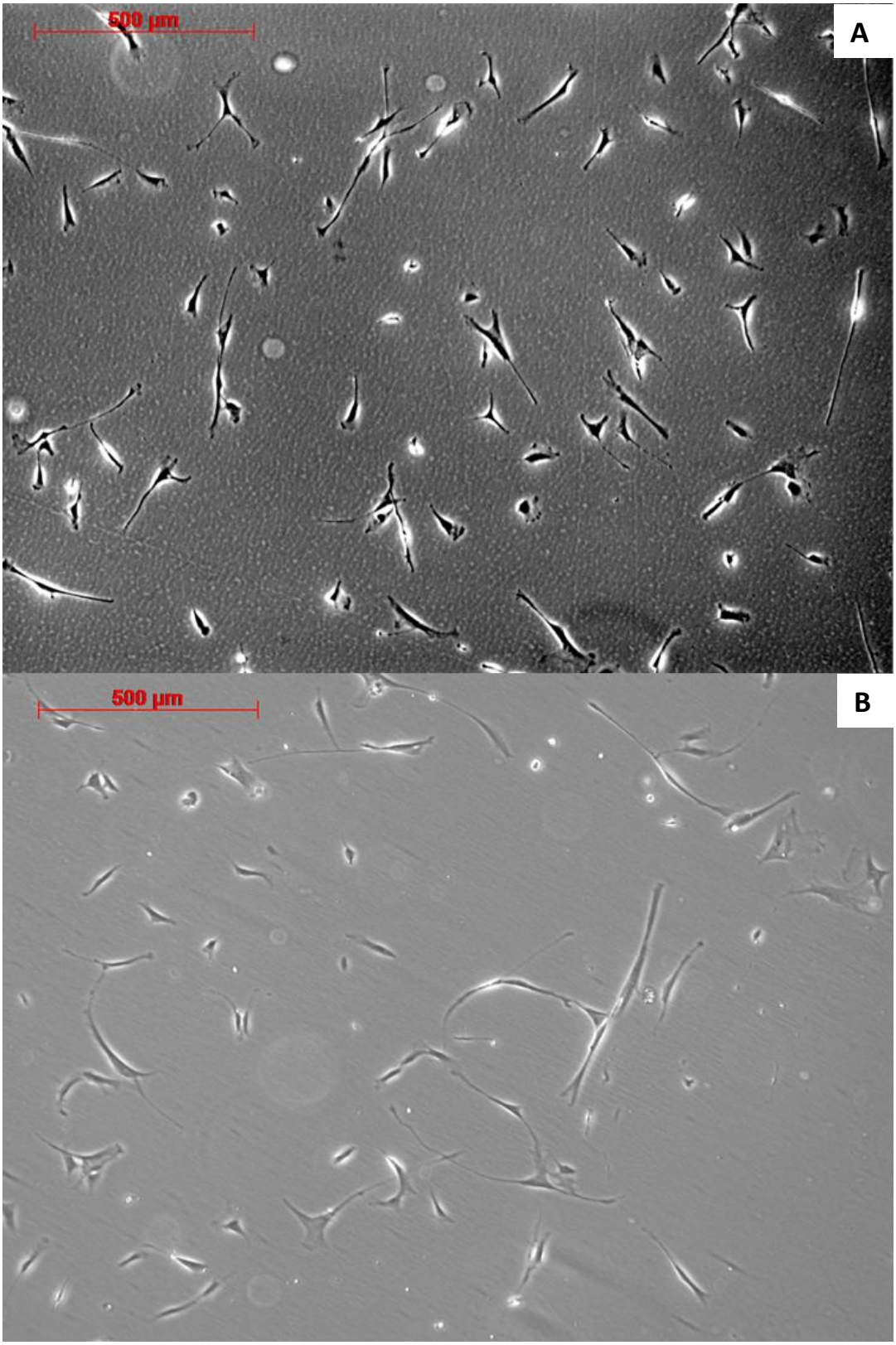

Figure 4.9 Comparison of healthy (A) and aneurysmal (B) SMCs at 5× in T-25 flask

CHAPTER V

CONCLUSIONS AND RECOMMENDATIONS

5.1. Healthy SMCs within cocultures

This study is based on the hypothesis that robust synthesis, organization and maturation of elastin and GAGs within adult blood vessels could be accomplished, on demand, by exogenously delivering NO cues which proffer developmental signals and stimulate the intrinsic elastogenesis capability of adult human aortic SMCs. Accordingly, a novel biomimetic, 3D cellular engineering approach has been developed and tested to evaluate the stand-alone and synergistic effects of NO and EC cocultures on the synthesis and deposition of matrix proteins on demand, which has not been attempted earlier. The following are the key conclusions from this study:

- We have shown that in the cases of both HA-SMCs cultured alone and in cocultures with HA-ECs, there is a suppression of the HA-SMC proliferation as

the dose of GSNO increased. This trend is not followed by the HA-EC cultures under the influence of GSNO.

- GSNO also encouraged multi-fold increases in the total ECM protein synthesis deposited into the cell matrix as well as released into the pooled media, with the most upregulation occurring at the 100 nM dose of GSNO.
- In general, addition of GSNO promoted increases in the ECM protein (elastin, GAGs, HA, and LOX) release as well as deposition into the cell matrix.
- The benefits of GSNO further increased in the presence of HA-EC cocultures.
- The matrix metalloproteinases that regulate the ECM protein of the vascular tissue and their inhibitors have also been affected by both the exogenously delivered GSNO and the HA-EC coculture. For the most part these enzymes as well as their inhibitors increased in the presence of GSNO and even more so under coculture conditions except for MMP-2 in the absence of coculture.
- Immunofluorescence labeling of both elastin and LOX qualitatively supports the deposition within cell matrices as quantified from biochemical assays. The staining for fibrillin could be seen modestly in all the cases, and it was predominately confined to the periphery of the cells.

5.2. Aneurysmal SMC in 2D and 3D cultures

- The proliferation of diseased aneurysmal HA-SMCs was suppressed in the presence of 100 nM GSNO in both 2D and 3D cultures.
- The total protein synthesized by the diseased cells (deposited and released into the pooled media) in both 2D and 3D cultures increased with the addition of 100 nM

GSNO. Also there was a significant upregulation of protein synthesis in the 3D cultures compared to the 2D cultures.

- The general trend of the specific ECM proteins studied (elastin, GAGs, HAs, and LOX) show a general upregulation in the presence of 100 nM GSNO. The trends showed on average a significant larger protein synthesis in 3D cultures than the 2D cultures.
- With the addition of 100 nM GSNO, the release of MMP-2, 9, and TIMP-1 showed a significant increase in the 2D cultures. As for the 3D cultures, there was only a significant increase in the presence of GSNO for the MMP-2 and TIMP-1. Finally, in the presence of GSNO, the values of MMP-2, 9, and TIMP-1 in 3D cultures were significantly larger than their 2D counterparts.
- Immunofluorescence labeling of both elastin and LOX qualitatively supports the deposition within cell matrices as previously discussed. The staining for fibrillin could be seen modestly in all cases it was predominately confined to the periphery of the cells.
- Overall the addition of GSNO significantly upregulates the ECM proteins necessary for homeostasis of diseased smooth muscle tissue. The overall proliferation and protein creation is minimal when compared to that of healthy tissue, so either higher concentrations of GSNO are needed, or more treatment time is necessary to return normal function to diseased HA-SMCs.
- The overall dimensions of the diseased cells in 2D were larger than the healthy SMCs, which can possibly explain the low amount of ECM release and deposition in the diseased assays when compared to the healthy experiments.

- ECM data obtained in aneurysm cell lines is much lower than the values obtained in healthy SMCs even though they follow similar trends.

5.3. Recommendations

The following are recommendations for future studies to further understand the effects of both nitric oxide as well as other possible factors in synthesis and regulation of vascular smooth muscle tissue.

- Test the role of fluid flow on cell behavior through a pulsatile pump attached to the described microfluidic device.
- Investigate the role of ECM microenvironment on cell migration, proliferation and matrix remodeling.
- Study the matrix synthesis and deposition by diseased adult human aortic smooth muscle cells within 3D biomimetic cocultures under the influence of nitric oxide.
- Relevant drug and toxicology screening, tissue engineering and regenerative medicine therapies, as well as vascular disease remodeling *in vivo*.

BIBLIOGRAPHY

1. Seeley RR, Tate P, Stephens TD. *Anatomy & Physiology*. 8th ed. Dubuque, IA: McGraw-Hill; 2008.

2. Representative images for our laboratory's smooth muscle cell research. *City Univ New York*. Available at: http://bme.ccny.cuny.edu/faculty/jtarbell/SMC images.htm. Accessed April 1, 2014.

3. Miner EC, Miller WL. A look between the cardiomyocytes: the extracellular matrix in heart failure. *Mayo Clin Proc*. 2006;81(1):71-6. doi:10.4065/81.1.71.

4. Pelouch V, Dixon IMC, Golfman L, Beamish RE, Dhalla NS. Role of extracellular matrix proteins in heart function. *Mol Cell Biochem*. 1993;129(2):101-120. doi:10.1007/BF00926359.

5. Bashey RI, Martinez-Hernandez A, Jimenez SA. Isolation, characterization, and localization of cardiac collagen type VI. Associations with other extracellular matrix components. *Circ Res*. 1992;70(5):1006-17. Available at: http://www.ncbi.nlm.nih.gov/pubmed/1568294. Accessed April 3, 2014.

6. Alberts B, Johnson A, Lewis J et al. *Molecular Biology of the Cell*. 4th ed. New York: Garland Science; 2002. Available at: http://www.ncbi.nlm.nih.gov/books/NBK26810/.

7. Weber KT, Sun Y, Tyagi SC, Cleutjens JP. Collagen network of the myocardium: function, structural remodeling and regulatory mechanisms. *J Mol Cell Cardiol*. 1994;26(3):279-92. doi:10.1006/jmcc.1994.1036.

8. Bax NAM, van Marion MH, Shah B, Goumans M-J, Bouten CVC, van der Schaft DWJ. Matrix production and remodeling capacity of cardiomyocyte progenitor cells during in vitro differentiation. *J Mol Cell Cardiol*. 2012;53(4):497-508. doi:10.1016/j.yjmcc.2012.07.003.

9. Alberts B. *Essential Cell Biology*. 3rd ed. New York: Garland Science; 2009.

10. Huynh MB, Morin C, Carpentier G, et al. Age-related changes in rat myocardium involve altered capacities of glycosaminoglycans to potentiate growth factor functions and heparan sulfate-altered sulfation. *J Biol Chem*. 2012;287(14):11363-73. doi:10.1074/jbc.M111.335901.

11. Wagenseil JE, Mecham RP. New insights into elastic fiber assembly. *Birth Defects Res C Embryo Today*. 2007;81(4):229-40. doi:10.1002/bdrc.20111.

12. Wagenseil JE, Mecham RP. Vascular extracellular matrix and arterial mechanics. *Physiol Rev*. 2009;89(3):957-89. doi:10.1152/physrev.00041.2008.

13. Fitzsimons C, Shanahan C. Vascular extracellular matrix. *Pan Vasc Med Integr Clin Manag*. 1972:217-226. Available at: http://link.springer.com/chapter/10.1007/978-3-642-56225-9_13#page-1.

14. Patel A, Fine B, Sandig M, Mequanint K. Elastin biosynthesis: The missing link in tissue-engineered blood vessels. *Cardiovasc Res*. 2006;71(1):40-9. doi:10.1016/j.cardiores.2006.02.021.

15. LOX lysyl oxidase [Homo sapiens (human)]. *Natl Cent Biotechnol Inf*. 2014. Available at: http://www.ncbi.nlm.nih.gov/gene?Db=gene&Cmd=ShowDetailView&TermToSearch=4015. Accessed March 28, 2014.

16. Ross R. Cell biology of atherosclerosis. *Annu Rev Physiol*. 1995;57:791-804. doi:10.1146/annurev.ph.57.030195.004043.

17. Aneurysm. *Encycl Sci*. Available at: http://www.daviddarling.info/encyclopedia/A/aneurysm.html.

18. Rosenbloom J, Abrams WR, Mecham R. Extracellular matrix 4: the elastic fiber. *FASEB J*. 1993;7(13):1208-18. Available at: http://www.ncbi.nlm.nih.gov/pubmed/8405806. Accessed April 3, 2014.

19. Kähäri VM, Chen YQ, Bashir MM, Rosenbloom J, Uitto J. Tumor necrosis factor-alpha down-regulates human elastin gene expression. Evidence for the role of AP-1 in the suppression of promoter activity. *J Biol Chem*. 1992;267(36):26134-41. Available at: http://www.ncbi.nlm.nih.gov/pubmed/1281483. Accessed April 3, 2014.

20. Galis ZS, Khatri JJ. Matrix Metalloproteinases in Vascular Remodeling and Atherogenesis: The Good, the Bad, and the Ugly. *Circ Res*. 2002:251-262. doi:0.1161/hh0302.105345.

21. Mecham RP, Broekelmann TJ, Fliszar CJ, Shapiro SD, Welgus HG, Senior RM. Elastin degradation by matrix metalloproteinases. Cleavage site specificity and mechanisms of elastolysis. *J Biol Chem*. 1997;272(29):18071-6. Available at: http://www.ncbi.nlm.nih.gov/pubmed/9218437. Accessed April 3, 2014.

22. Petersen E, Wagberg F, Angquist KA. Activity of matrix metalloproteinase-2 and -9 in abdominal aortic aneurysms. *Eur J Vasc Endovasc Surg*. 2000:457.

23. Lindholt JS, Jørgensen B, Klitgaard NA, Henneberg EW. Systemic levels of cotinine and elastase, but not pulmonary function, are associated with the

progression of small abdominal aortic aneurysms. *Eur J Vasc Endovasc Surg*. 2003;26(4):418-22. Available at: http://www.ncbi.nlm.nih.gov/pubmed/14512006. Accessed April 3, 2014.

24. Sandberg LB, Soskel NT, Leslie JG. Elastin structure, biosynthesis, and relation to disease states. *N Engl J Med*. 1981;304(10):566-79. doi:10.1056/NEJM198103053041004.

25. Raines EW, Ross R. Smooth muscle cells and the pathogenesis of the lesions of atherosclerosis. *Br Heart J*. 1993;69(1 Suppl):S30-7. Available at: http://www.pubmedcentral.nih.gov/articlerender.fcgi?artid=1025256&tool=pmcentrez&rendertype=abstract. Accessed April 3, 2014.

26. Brooke BS, Bayes-Genis A, Li DY. New insights into elastin and vascular disease. *Trends Cardiovasc Med*. 2003;13(5):176-81. Available at: http://www.ncbi.nlm.nih.gov/pubmed/12837579. Accessed April 3, 2014.

27. Keating M. Elastin and vascular disease. *Trends Cardiovasc Med*. 1994;4(4):165-9. doi:10.1016/1050-1738(94)90053-1.

28. Selle JG, Robicsek F, Daugherty HK, Cook JW. Thoracoabdominal aortic aneurysms. A review and current status. *Ann Surg*. 1979;189(2):158-64. Available at: http://www.pubmedcentral.nih.gov/articlerender.fcgi?artid=1397025&tool=pmcentrez&rendertype=abstract. Accessed April 3, 2014.

29. Guo D-C, Papke CL, He R, Milewicz DM. Pathogenesis of thoracic and abdominal aortic aneurysms. *Ann N Y Acad Sci*. 2006;1085:339-52. doi:10.1196/annals.1383.013.

30. Wang TJ, Vasan RS. Epidemiology of uncontrolled hypertension in the United States. *Circulation*. 2005;112(11):1651-62. doi:10.1161/CIRCULATIONAHA.104.490599.

31. Sutton-Tyrrell K, Najjar SS, Boudreau RM, et al. Elevated aortic pulse wave velocity, a marker of arterial stiffness, predicts cardiovascular events in well-functioning older adults. *Circulation*. 2005;111(25):3384-90. doi:10.1161/CIRCULATIONAHA.104.483628.

32. Li RX, Luo J, Balaram SK, Chaudhry FA, Shahmirzadi D, Konofagou EE. Pulse wave imaging in normal, hypertensive and aneurysmal human aortas in vivo: a feasibility study. *Phys Med Biol*. 2013;58(13):4549-62. doi:10.1088/0031-9155/58/13/4549.

33. Maldonado T. Abdominal Aortic Aneurysm: The Silent Killer. *Long Island Press*. http://archive.longislandpress.com/2010/08/17/abdominal-aortic-aneurysm-the-silent-killer/. Published August 17, 2010.

34. Kleinstreuer C, Li Z, Farber MA. Fluid-structure interaction analyses of stented abdominal aortic aneurysms. *Annu Rev Biomed Eng*. 2007;9:169-204. doi:10.1146/annurev.bioeng.9.060906.151853.

35. Stather PW, Dattani N, Bown MJ, Earnshaw JJ, Lees TA. International variations in AAA screening. *Eur J Vasc Endovasc Surg*. 2013;45(3):231-4. doi:10.1016/j.ejvs.2012.12.013.

36. Stankus JJ, Guan J, Wagner WR. Fabrication of biodegradable elastomeric scaffolds with sub-micron morphologies. *J Biomed Mater Res A*. 2004;70(4):603-14. doi:10.1002/jbm.a.30122.

37. STEHBENS WE. History of aneurysms. *Med Hist*. 1958;2(4):274-80. Available at: http://www.pubmedcentral.nih.gov/articlerender.fcgi?artid=1034418&tool=pmcentrez&rendertype=abstract. Accessed April 3, 2014.

38. Livesay JJ. Landmarks In Cardiac Surgery. *Texas Hear Inst J*. 2000;27(2):222. Available at: http://www.ncbi.nlm.nih.gov/pmc/articles/PMC101064/. Accessed April 3, 2014.

39. Matas R. An operation for the radical cure of aneurism based upon arteriorraphy. *Ann Surg*. 1903:161-196.

40. Livesay JJ, Messner GN, Vaughn WK. Milestones in the treatment of aortic aneurysm: Denton A. Cooley, MD, and the Texas Heart Institute. *Tex Heart Inst J*. 2005;32(2):130-4. Available at: http://www.pubmedcentral.nih.gov/articlerender.fcgi?artid=1163455&tool=pmcentrez&rendertype=abstract. Accessed April 3, 2014.

41. COOLEY DA, DE BAKEY ME. Surgical considerations of intrathoracic aneurysms of the aorta and great vessels. *Ann Surg*. 1952;135(5):660-80. Available at: http://www.pubmedcentral.nih.gov/articlerender.fcgi?artid=1802172&tool=pmcentrez&rendertype=abstract. Accessed April 3, 2014.

42. Barker WF. *The Arteries*. Austin, TX: R.G. Landes; 1992.

43. Bakey ME De. SUCCESSFUL RESECTION OF ANEURYSM OF DISTAL AORTIC ARCH AND REPLACEMENT BY GRAFT. *J Am Med Assoc*. 1954;155(16):1398. doi:10.1001/jama.1954.03690340020007.

44. COOLEY DA, DEBAKEY ME. Resection of the thoracic aorta with replacement by homograft for aneurysms and constrictive lesions. *J Thorac Surg*. 1955;29(1):66-100; discussion, 100-4. Available at: http://www.ncbi.nlm.nih.gov/pubmed/13222475. Accessed April 3, 2014.

45. Cooley DA, Mahaffey DE. Total excision of the aortic arch for aneurysm. *Surg Gynecol Obstet*. 1955;(101):667-672.

46. DE BAKEY ME, COOLEY DA, CREECH O. Surgical considerations of dissecting aneurysm of the aorta. *Ann Surg*. 1955;142(4):586-610; discussion, 611-2. Available at: http://www.pubmedcentral.nih.gov/articlerender.fcgi?artid=1465201&tool=pmcentrez&rendertype=abstract. Accessed April 3, 2014.

47. Cooley DA. RESECTION OF ENTIRE ASCENDING AORTA IN FUSIFORM ANEURYSM USING CARDIAC BYPASS. *J Am Med Assoc*. 1956;162(12):1158. doi:10.1001/jama.1956.72970290003013a.

48. Lewis CTP, Cooley DA, Murphy MC, Talledo O, Vega D. Surgical repair of aortic root aneurysms in 280 patients. *Ann Thorac Surg*. 1992;53(1):38-46. doi:10.1016/0003-4975(92)90755-S.

49. Livesay JJ, Cooley DA, Reul GJ, et al. Resection of aortic arch aneurysms: a comparison of hypothermic techniques in 60 patients. *Ann Thorac Surg*. 1983;36(1):19-28. Available at: http://www.ncbi.nlm.nih.gov/pubmed/6222711. Accessed April 3, 2014.

50. Wukasch DC, Cooley DA, Bennett JG, Gontijo B, Bongiorno FP. Results of a new Meadox-Cooley double velour dacron graft for arterial reconstruction. *J Cardiovasc Surg (Torino)*. 20(3):249-60. Available at: http://www.ncbi.nlm.nih.gov/pubmed/156190. Accessed April 3, 2014.

51. Cooley DA, Romagnoli A, Milam JD, Bossart MI. A method of preparing woven Dacron aortic grafts to prevent interstitial hemorrhage. *Cardiovasc Dis*. 1981;8(1):48-52. Available at: http://www.pubmedcentral.nih.gov/articlerender.fcgi?artid=287898&tool=pmcentrez&rendertype=abstract. Accessed April 3, 2014.

52. Abdominal Aortic Aneurysm and Treatment. *Northwest Meml Hosp*. 2013. Available at: http://www.nmh.org/nm/vascular-disease-abdominal-aortic-aneurysm-and-treatment. Accessed March 31, 2014.

53. Sluzewski M, van Rooij WJ, Slob MJ, Bescós JO, Slump CH, Wijnalda D. Relation between aneurysm volume, packing, and compaction in 145 cerebral aneurysms treated with coils. *Radiology*. 2004;231(3):653-8. doi:10.1148/radiol.2313030460.

54. Drugs for Lipids. *Treat Guidel Med Lett*. 2011;9(103):13-20.

55. Drugs for hypertension. *Treat Guidel Med Lett*. 2012;10(113):1-10.

56. Weinberg CB, Bell E. A blood vessel model constructed from collagen and cultured vascular cells. *Science*. 1986;231(4736):397-400. Available at: http://www.ncbi.nlm.nih.gov/pubmed/2934816. Accessed April 3, 2014.

57. Edelman ER. Vascular tissue engineering : designer arteries. *Circ Res*. 85(12):1115-7. Available at: http://www.ncbi.nlm.nih.gov/pubmed/10590236. Accessed April 3, 2014.

58. L'Heureux N, Pâquet S, Labbé R, Germain L, Auger FA. A completely biological tissue-engineered human blood vessel. *FASEB J*. 1998;12(1):47-56. Available at: http://www.ncbi.nlm.nih.gov/pubmed/9438410. Accessed March 27, 2014.

59. Ravi S, Chaikof EL. Biomaterials for vascular tissue engineering. *Regen Med*. 2010;5(1):107-20. doi:10.2217/rme.09.77.

60. Rumisek JD, Wade CE, Brooks DE, Okerberg C V, Barry MJ, Clarke JS. Heat-denatured albumin-coated Dacron vascular grafts: physical characteristics and in vivo performance. *J Vasc Surg*. 1986;4(2):136-43. Available at: http://www.ncbi.nlm.nih.gov/pubmed/2942709. Accessed April 3, 2014.

61. Williams SK, Rose DG, Jarrell BE. Microvascular endothelial cell sodding of ePTFE vascular grafts: improved patency and stability of the cellular lining. *J Biomed Mater Res*. 1994;28(2):203-12. doi:10.1002/jbm.820280210.

62. Mann MJ, Gibbons GH, Kernoff RS, et al. Genetic engineering of vein grafts resistant to atherosclerosis. *Proc Natl Acad Sci U S A*. 1995;92(10):4502-6. Available at: http://www.pubmedcentral.nih.gov/articlerender.fcgi?artid=41972&tool=pmcentrez&rendertype=abstract. Accessed April 3, 2014.

63. Campbell JH, Efendy JL, Campbell GR. Novel vascular graft grown within recipient's own peritoneal cavity. *Circ Res*. 85(12):1173-8. Available at: http://www.ncbi.nlm.nih.gov/pubmed/10590244. Accessed April 3, 2014.

64. Niklason LE. Functional Arteries Grown in Vitro. *Science (80-).* 1999;284(5413):489-493. doi:10.1126/science.284.5413.489.

65. Gross SS, Wolin MS. Nitric oxide: pathophysiological mechanisms. *Annu Rev Physiol*. 1995;57:737-69. doi:10.1146/annurev.ph.57.030195.003513.

66. Palmer RM, Ashton DS, Moncada S. Vascular endothelial cells synthesize nitric oxide from L-arginine. *Nature*. 1988;333(6174):664-6. doi:10.1038/333664a0.

67. Palmer RM, Rees DD, Ashton DS, Moncada S. L-arginine is the physiological precursor for the formation of nitric oxide in endothelium-dependent relaxation. *Biochem Biophys Res Commun*. 1988;153(3):1251-6. Available at: http://www.ncbi.nlm.nih.gov/pubmed/3390182. Accessed April 3, 2014.

68. Knowles RG, Palacios M, Palmer RM, Moncada S. Formation of nitric oxide from L-arginine in the central nervous system: a transduction mechanism for stimulation of the soluble guanylate cyclase. *Proc Natl Acad Sci U S A*. 1989;86(13):5159-62. Available at: http://www.pubmedcentral.nih.gov/articlerender.fcgi?artid=297577&tool=pmcentrez&rendertype=abstract. Accessed April 3, 2014.

69. Moncada S, Palmer RM, Higgs EA. Biosynthesis of nitric oxide from L-arginine. A pathway for the regulation of cell function and communication. *Biochem Pharmacol*. 1989;38(11):1709-15. Available at: http://www.ncbi.nlm.nih.gov/pubmed/2567594. Accessed April 3, 2014.

70. Moncada S, Palmer RM, Higgs EA. Nitric oxide: physiology, pathophysiology, and pharmacology. *Pharmacol Rev*. 1991;43(2):109-42. Available at: http://www.ncbi.nlm.nih.gov/pubmed/1852778. Accessed March 20, 2014.

71. Palmer RM, Ferrige AG, Moncada S. Nitric oxide release accounts for the biological activity of endothelium-derived relaxing factor. *Nature*. 327(6122):524-6. doi:10.1038/327524a0.

72. Moroi M, Zhang L, Yasuda T, et al. Interaction of genetic deficiency of endothelial nitric oxide, gender, and pregnancy in vascular response to injury in mice. *J Clin Invest*. 1998;101(6):1225-32. doi:10.1172/JCI1293.

73. Steudel W, Scherrer-Crosbie M, Bloch KD, et al. Sustained pulmonary hypertension and right ventricular hypertrophy after chronic hypoxia in mice with congenital deficiency of nitric oxide synthase 3. *J Clin Invest*. 1998;101(11):2468-77. doi:10.1172/JCI2356.

74. Sugitani H, Wachi H, Tajima S, Seyama Y. Nitric oxide stimulates elastin expression in chick aortic smooth muscle cells. *Biol Pharm Bull*. 2001;24(5):461-4. Available at: http://www.ncbi.nlm.nih.gov/pubmed/11379760. Accessed April 3, 2014.

75. Girard P, Potier P. NO, thiols and disulfides. *FEBS Lett*. 1993;320(1):7-8. Available at: http://www.ncbi.nlm.nih.gov/pubmed/8462679. Accessed May 4, 2014.

76. Myers PR, Minor RL, Guerra R, Bates JN, Harrison DG. Vasorelaxant properties of the endothelium-derived relaxing factor more closely resemble S-

nitrosocysteine than nitric oxide. *Nature*. 1990;345(6271):161-3. doi:10.1038/345161a0.

77. Konorev E, Tarpey M, Joseph J, Baker J, Kalyanaraman B. S-nitrosoglutathione improves functional recovery in the isolated rat heart after cardioplegic ischemic arrest-evidence for a cardioprotective effect of nitric oxide. *J Pharmacol Exp Ther*. 1995;274(1):200-206. Available at: http://jpet.aspetjournals.org/content/274/1/200.abstract?ijkey=c57d01182cbef802a0ed6e6ccbc49906822ec91d&keytype2=tf_ipsecsha. Accessed May 6, 2014.

78. Arnelle DR, Stamler JS. NO+, NO, and NO- donation by S-nitrosothiols: implications for regulation of physiological functions by S-nitrosylation and acceleration of disulfide formation. *Arch Biochem Biophys*. 1995;318(2):279-85. doi:10.1006/abbi.1995.1231.

79. Singh RJ, Hogg N, Joseph J, Kalyanaraman B. Mechanism of Nitric Oxide Release from S-Nitrosothiols. *J Biol Chem*. 1996;271(31):18596-18603. Available at: http://www.jbc.org/content/271/31/18596.long. Accessed May 4, 2014.

80. Gaston B, Reilly J, Drazen JM, et al. Endogenous nitrogen oxides and bronchodilator S-nitrosothiols in human airways. *Proc Natl Acad Sci*. 1993;90(23):10957-10961. doi:10.1073/pnas.90.23.10957.

81. Clancy RM, Levartovsky D, Leszczynska-Piziak J, Yegudin J, Abramson SB. Nitric oxide reacts with intracellular glutathione and activates the hexose monophosphate shunt in human neutrophils: evidence for S-nitrosoglutathione as a bioactive intermediary. *Proc Natl Acad Sci*. 1994;91(9):3680-3684. doi:10.1073/pnas.91.9.3680.

82. Nikitovic D, Holmgren A. S-nitrosoglutathione is cleaved by the thioredoxin system with liberation of glutathione and redox regulating nitric oxide. *J Biol Chem*. 1996;271(32):19180-5. Available at: http://www.ncbi.nlm.nih.gov/pubmed/8702596. Accessed April 5, 2014.

83. S-Nitrosoglutathione. Available at: http://www.sigmaaldrich.com/catalog/product/sigma/n4148?lang=en&region=US. Accessed May 4, 2014.

84. Stuehr DJ, Marletta MA. Mammalian nitrate biosynthesis: mouse macrophages produce nitrite and nitrate in response to Escherichia coli lipopolysaccharide. *Proc Natl Acad Sci*. 1985;82(22):7738-7742. doi:10.1073/pnas.82.22.7738.

85. Stamler JS. Redox signaling: nitrosylation and related target interactions of nitric oxide. *Cell*. 1994;78(6):931-6. Available at: http://www.ncbi.nlm.nih.gov/pubmed/7923362. Accessed May 6, 2014.

86. Schmidt HH, Walter U. NO at work. *Cell*. 1994;78(6):919-25. Available at: http://www.ncbi.nlm.nih.gov/pubmed/7923361. Accessed May 6, 2014.

87. Nathan C, Xie QW. Nitric oxide synthases: roles, tolls, and controls. *Cell*. 1994;78(6):915-8. Available at: http://www.ncbi.nlm.nih.gov/pubmed/7522969. Accessed May 6, 2014.

88. Hogg N, Singh RJ, Kalyanaraman B. The role of glutathione in the transport and catabolism of nitric oxide. *FEBS Lett*. 1996;382(3):223-8. Available at: http://www.ncbi.nlm.nih.gov/pubmed/8605974. Accessed May 6, 2014.

89. Kothapalli CR, Taylor PM, Smolenski RT, Yacoub MH, Ramamurthi A. Transforming growth factor beta 1 and hyaluronan oligomers synergistically enhance elastin matrix regeneration by vascular smooth muscle cells. *Tissue Eng Part A*. 2009;15(3):501-11. doi:10.1089/ten.tea.2008.0040.

90. Labarca C, Paigen K. A simple, rapid, and sensitive DNA assay procedure. *Anal Biochem*. 1980;102(2):344-352. doi:10.1016/0003-2697(80)90165-7.

91. Mancuso C, Bonsignore A, Di Stasio E, Mordente A, Motterlini R. Bilirubin and S-nitrosothiols interaction: evidence for a possible role of bilirubin as a scavenger of nitric oxide. *Biochem Pharmacol*. 2003;66(12):2355-63. Available at: http://www.ncbi.nlm.nih.gov/pubmed/14637193. Accessed April 5, 2014.

92. Isenberg JS, Wink DA, Roberts DD. Thrombospondin-1 antagonizes nitric oxide-stimulated vascular smooth muscle cell responses. *Cardiovasc Res*. 2006;71(4):785-93. doi:10.1016/j.cardiores.2006.05.024.

93. Snyder AH, McPherson ME, Hunt JF, Johnson M, Stamler JS, Gaston B. Acute effects of aerosolized S-nitrosoglutathione in cystic fibrosis. *Am J Respir Crit Care Med*. 2002;165(7):922-6. doi:10.1164/ajrccm.165.7.2105032.

94. Yu H, Payne TJ, Mohanty DK. Effects of slow, sustained, and rate-tunable nitric oxide donors on human aortic smooth muscle cells proliferation. *Chem Biol Drug Des*. 2011;78(4):527-34. doi:10.1111/j.1747-0285.2011.01174.x.

95. Singh SP, Wishnok JS, Keshive M, Deen WM, Tannenbaum SR. The chemistry of the S-nitrosoglutathione/glutathione system. *Proc Natl Acad Sci*. 1996;93(25):14428-14433. doi:10.1073/pnas.93.25.14428.

96. Yang W, Ando J, Korenaga R, Toyo-oka T, Kamiya A. Exogenous nitric oxide inhibits proliferation of cultured vascular endothelial cells. *Biochem Biophys Res Commun*. 1994;203(2):1160-7. Available at: http://www.ncbi.nlm.nih.gov/pubmed/7916569. Accessed April 5, 2014.

97. Jeremy J. Nitric oxide and the proliferation of vascular smooth muscle cells. *Cardiovasc Res*. 1999;43(3):580-594. doi:10.1016/S0008-6363(99)00171-6.

98. Fillinger MF, O'Connor SE, Wagner RJ, Cronenwett JL. The effect of endothelial cell coculture on smooth muscle cell proliferation. *J Vasc Surg*. 1993;17(6):1058-67; discussion 1067-8. Available at: http://www.ncbi.nlm.nih.gov/pubmed/8505784. Accessed April 5, 2014.

99. Kolpakov V, Gordon D, Kulik TJ. Nitric oxide-generating compounds inhibit total protein and collagen synthesis in cultured vascular smooth muscle cells. *Circ Res*. 1995;76(2):305-9. Available at: http://www.ncbi.nlm.nih.gov/pubmed/7834842. Accessed April 5, 2014.

100. Garg UC, Hassid A. Mechanisms of nitrosothiol-induced antimitogenesis in aortic smooth muscle cells. *Eur J Pharmacol*. 1993;237(2-3):243-9. Available at: http://www.ncbi.nlm.nih.gov/pubmed/7689974. Accessed April 5, 2014.

101. Curran RD, Ferrari FK, Kispert PH, et al. Nitric oxide and nitric oxide-generating compounds inhibit hepatocyte protein synthesis. *FASEB J*. 1991;5(7):2085-92. Available at: http://www.ncbi.nlm.nih.gov/pubmed/1707021. Accessed April 5, 2014.

102. Bashur CA, Venkataraman L, Ramamurthi A. Tissue engineering and regenerative strategies to replicate biocomplexity of vascular elastic matrix assembly. *Tissue Eng Part B Rev*. 2012;18(3):203-17. doi:10.1089/ten.TEB.2011.0521.

103. Sivaraman B, Bashur CA, Ramamurthi A. Advances in biomimetic regeneration of elastic matrix structures. *Drug Deliv Transl Res*. 2012;2(5):323-350. doi:10.1007/s13346-012-0070-6.

104. Kothapalli CR, Ramamurthi A. Benefits of concurrent delivery of hyaluronan and IGF-1 cues to regeneration of crosslinked elastin matrices by adult rat vascular cells. *J Tissue Eng Regen Med*. 2(2-3):106-16. doi:10.1002/term.70.

105. Kothapalli CR, Ramamurthi A. Biomimetic regeneration of elastin matrices using hyaluronan and copper ion cues. *Tissue Eng Part A*. 2009;15(1):103-13. doi:10.1089/ten.tea.2007.0390.

106. Kothapalli CR, Ramamurthi A. Copper nanoparticle cues for biomimetic cellular assembly of crosslinked elastin fibers. *Acta Biomater*. 2009;5(2):541-53. doi:10.1016/j.actbio.2008.09.004.

107. Kothapalli CR, Ramamurthi A. Lysyl oxidase enhances elastin synthesis and matrix formation by vascular smooth muscle cells. *J Tissue Eng Regen Med*. 2009;3(8):655-61. doi:10.1002/term.214.

108. Lin S, Sandig M, Mequanint K. Three-dimensional topography of synthetic scaffolds induces elastin synthesis by human coronary artery smooth muscle cells. *Tissue Eng Part A*. 2011;17(11-12):1561-71. doi:10.1089/ten.TEA.2010.0593.

109. Lin S, Mequanint K. The role of Ras-ERK-IL-1β signaling pathway in upregulation of elastin expression by human coronary artery smooth muscle cells cultured in 3D scaffolds. *Biomaterials*. 2012;33(29):7047-56. doi:10.1016/j.biomaterials.2012.06.044.

110. Venkataraman L, Ramamurthi A. Induced elastic matrix deposition within three-dimensional collagen scaffolds. *Tissue Eng Part A*. 2011;17(21-22):2879-89. doi:10.1089/ten.TEA.2010.0749.

111. Venkataraman L, Bashur CA, Ramamurthi A. Impact of Cyclic Stretch on Induced Elastogenesis Within Collagenous Conduits. *Tissue Eng Part A*. 2014. doi:10.1089/ten.TEA.2013.0294.

112. Mourão PA, Luz MR, Borojevic R. Sulfated glycosaminoglycans synthesized by human smooth muscle cells isolated from different organs. *Biochim Biophys Acta*. 1986;881(3):321-9. Available at: http://www.ncbi.nlm.nih.gov/pubmed/3083867. Accessed April 5, 2014.

113. Suarez ER, Nohara AS, Mataveli FD, de Matos LL, Nader HB, Pinhal MAS. Glycosaminoglycan synthesis and shedding induced by growth factors are cell and compound specific. *Growth Factors*. 2007;25(1):50-9. doi:10.1080/08977190701272701.

114. Dey NB, Lincoln TM. Possible involvement of Cyclic-GMP-dependent protein kinase on matrix metalloproteinase-2 expression in rat aortic smooth muscle cells. *Mol Cell Biochem*. 2012;368(1-2):27-35. doi:10.1007/s11010-012-1339-2.

115. Crowther M, Goodall S, Jones JL, Bell PR, Thompson MM. Increased matrix metalloproteinase 2 expression in vascular smooth muscle cells cultured from abdominal aortic aneurysms. *J Vasc Surg*. 2000;32(3):575-83. doi:10.1067/mva.2000.108010.

116. Kothapalli CR, Gacchina CE, Ramamurthi A. Utility of hyaluronan oligomers and transforming growth factor-beta1 factors for elastic matrix regeneration by aneurysmal rat aortic smooth muscle cells. *Tissue Eng Part A*. 2009;15(11):3247-60. doi:10.1089/ten.TEA.2008.0593.

117. Simmers P, Gishto A, Kothapalli C. Nitric oxide stimulates matrix synthesis and deposition by adult human aortic smooth muscle cells within 3D biomimetic cocultures. *Rev*. 2014.

118. Ishii Y, Ogura T, Tatemichi M, Fujisawa H, Otsuka F, Esumi H. Induction of matrix metalloproteinase gene transcription by nitric oxide and mechanisms of MMP-1 gene induction in human melanoma cell lines. *Int J Cancer*. 2003;103(2):161-8. doi:10.1002/ijc.10808.

119. Greenlee KJ, Werb Z, Kheradmand F. Matrix metalloproteinases in lung: multiple, multifarious, and multifaceted. *Physiol Rev*. 2007;87(1):69-98. doi:10.1152/physrev.00022.2006.